

DOE/ER/40762-164
UMDPP#99-039
NT@UW-99-7
KRL MAP-239

Compton Scattering on the Deuteron in Baryon Chiral Perturbation Theory

S.R. Beane¹, M. Malheiro^{2,1},
D.R. Phillips^{3,1} and U. van Kolck^{4,3}

¹*Department of Physics,
University of Maryland, College Park, MD 20742
sbeane@physics.umd.edu*

²*Instituto de Física,
Universidade Federal Fluminense, 24210-340, Niterói, R.J., Brazil
mane@if.uff.br*

³*Department of Physics
University of Washington, Seattle, WA 98195-1560
phillips@dirac.phys.washington.edu*

⁴*Kellogg Radiation Laboratory, 106-38
California Institute of Technology, Pasadena, CA 91125
vankolck@krl.caltech.edu*

Abstract

Compton scattering on the deuteron is studied in the framework of baryon chiral perturbation theory to third order in small momenta, for photon energies of order the pion mass. The scattering amplitude is a sum of one- and two-nucleon mechanisms with no undetermined parameters. Our results are in good agreement with existing experimental data, and a prediction is made for higher-energy data being analyzed at SAL.

PACS nos.: 13.60.Fz, 12.39.Fe, 25.20.-x, 12.39.Pn, 21.45.+v

1 Introduction

Experimental facilities which accurately measure the energy of a photon beam using photon tagging have made possible a new generation of experiments which probe the low-energy structure of nucleons and nuclei. In particular, photon tagging can be used to measure Compton scattering on weakly-bound systems, since it facilitates the separation of elastic and inelastic cross sections. At sufficiently low energy ω the spin-averaged forward Compton scattering amplitude for any nucleus is, in the nuclear rest frame:

$$T(\omega) = -\frac{1}{4\pi}\vec{\epsilon}' \cdot \vec{\epsilon} \left(\frac{\mathcal{Z}^2 e^2}{AM} + (\alpha + \beta)\omega^2 + \dots \right), \quad (1)$$

where $\vec{\epsilon}$ and $\vec{\epsilon}'$ are the polarization vectors of the initial and final-state photons, $\mathcal{Z}e$ is the total charge of the nucleus, and AM is its total mass. The first term in this series is a consequence of gauge invariance, and is the Thomson limit for low-energy scattering on a target of mass number A and atomic number \mathcal{Z} . The coefficient of the second term is the sum of the target electric and magnetic polarizabilities, α and β , respectively. The polarizabilities can be separated by going to backward angles, which probes the difference, $\alpha - \beta$. The polarizabilities contain information about the electromagnetic structure of the target.

A number of recent experiments have focused on Compton scattering on the proton and on the deuteron. These experiments have already resulted in a wealth of new data on α_p and β_p , the proton electric and magnetic polarizabilities, and might yield information on α_n and β_n , the corresponding neutron quantities. These are basic low-energy hadron parameters which reflect the underlying QCD dynamics. In a simple quark model picture they contain averaged information about the charge and current distribution produced by the quarks inside the nucleon.

At energies well below the chiral symmetry breaking scale, $\Lambda_\chi \sim 4\pi f_\pi \sim M \sim m_\rho$, the electromagnetic interactions of pions and nucleons can be described systematically using an effective field theory. This effective field theory, known as chiral perturbation theory (χPT), reflects the observed QCD pattern of symmetry breaking; there is an approximate $SU(2)_L \times SU(2)_R$ symmetry which is spontaneously broken to $SU(2)_V$ (isospin). This pattern of spontaneous symmetry breaking gives rise to three Goldstone bosons which are identified with the pions. In the chiral limit pions interact only through derivative interactions. A finite pion mass reflects the nonvanishing current quark masses in QCD. χPT is a useful theory because pions interact only through vertices with a countable number of derivatives and/or insertions of the quark mass matrix; each power of the pion mass and each derivative count as one power of “small momenta”. Therefore S -matrix elements computed in χPT can be expressed as simultaneous expansions in powers of momenta and pion masses over the characteristic scale of physics that is not included explicitly in the effective theory:

$$\frac{Q}{\Lambda_\chi}, \quad (2)$$

taking Q to represent a “small momentum”: a momentum $p \ll \Lambda_\chi$ or a pion mass. Note that the dynamical effects of *all* mesons other than the pion are accounted for through local pionic operators. In the purest form of χPT , the coefficients of these operators are fit to one experiment and then used to predict other experiments. Hence χPT is a predictive theory. The machinery of χPT was originally developed for Goldstone boson interactions. However, it is straightforward to extend the machinery to include single-baryon processes, with the baryons treated as heavy, static objects. This subject is reviewed in great detail in Ref. [1].

Nucleon Compton scattering has been studied in χPT in Ref. [2], where the following results for the polarizabilities were obtained to order Q^3 :

$$\begin{aligned} \alpha_p = \alpha_n &= \frac{5e^2 g_A^2}{384\pi^2 f_\pi^2 m_\pi} = 12.2 \times 10^{-4} \text{ fm}^3; \\ \beta_p = \beta_n &= \frac{e^2 g_A^2}{768\pi^2 f_\pi^2 m_\pi} = 1.2 \times 10^{-4} \text{ fm}^3. \end{aligned} \quad (3)$$

Here we have used $g_A = 1.26$ for the axial coupling of the nucleon, and $f_\pi = 93$ MeV as the pion decay constant. Note that the polarizabilities are *predictions* of χPT at this order. The $O(Q^3)$ χPT predictions diverge in the chiral limit because they arise from pion loop effects. In less precise language, the power counting of χPT implies that polarizabilities are dominated by the dynamics of the long-ranged pion cloud surrounding the nucleon, rather than by short-range dynamics. The polarizabilities should thus provide a sensitive test of chiral dynamics.

At the next order in the chiral expansion, Q^4 , there are contributions to the polarizabilities from undetermined parameters which must be fixed independently [3]. These counterterms account for short-range contributions to the nucleon structure. This higher-order calculation will be discussed further below.

Recent experimental values for the proton polarizabilities are [4]¹

$$\begin{aligned} \alpha_p + \beta_p &= 13.23 \pm 0.86_{-0.49}^{+0.20} \times 10^{-4} \text{ fm}^3, \\ \alpha_p - \beta_p &= 10.11 \pm 1.74_{-0.86}^{+1.22} \times 10^{-4} \text{ fm}^3, \end{aligned} \quad (4)$$

where the first error is a combined statistical and systematic error, and the second set of errors comes from the theoretical model employed. We note that the value of $\alpha_p + \beta_p$

¹These are the result of a model-dependent fit to data from Compton scattering on the proton at several angles and at energies ranging from 33 to 309 MeV.

extracted from this multi-energy fit is consistent with the venerable Baldin sum rule [5]. These values are also in good agreement with the chiral perturbation theory predictions. The neutron polarizabilities are difficult to obtain experimentally and so the corresponding χPT prediction is not well tested. A dispersion sum rule can relate the sum of electric and magnetic polarizabilities to an integral of the deuteron photo-absorption cross section; with model-dependent assumptions about the size of the neutron contribution to the deuteron photo-absorption cross section, it has been found that [5]

$$\alpha_n + \beta_n = (14.40 \pm 0.66) \times 10^{-4} \text{ fm}^3. \quad (5)$$

Most direct information on α_n has been obtained by scattering neutrons on a heavy nucleus and examining the cross section as a function of energy. Currently there is much controversy over what result this technique gives for α_n . In Ref. [6] the value ²

$$\alpha_n = (12.6 \pm 1.5 \pm 2.0) \times 10^{-4} \text{ fm}^3 \quad (6)$$

was obtained, which disagrees considerably with the result of the experiment of Ref. [8],

$$\alpha_n = (0.6 \pm 5.0) \times 10^{-4} \text{ fm}^3. \quad (7)$$

Given this discrepancy, it is important to measure the electromagnetic neutron polarizabilities by other means. Compton scattering on a nuclear target is an obvious candidate. Quasi-free Compton scattering by the neutron in a deuteron target was reported in Ref. [9]. With the use of a theoretical model, the polarizability

$$\alpha_n = (10.7^{+3.3}_{-10.7}) \times 10^{-4} \text{ fm}^3 \quad (8)$$

was extracted. One difficulty with this extraction of the polarizability by scattering on a nuclear target lies in the absence of a large neutron contribution: for quasi-free scattering the cross section in the forward direction goes as $\sigma_n \sim (\alpha_n \omega^2)^2$ (where we have neglected the smaller magnetic polarizability) and is very small. Partly for this reason, attention has turned to other methods of extracting the neutron polarizabilities. It should be pointed out though that some authors argue that quasi-free photon-neutron scattering deserves renewed study [10].

One alternative to this quasi-free Compton scattering is coherent photon scattering on the deuteron. In this case, the cross section in the forward direction naively goes as:

$$\left. \frac{d\sigma}{d\Omega} \right|_{\theta=0} \sim (f_{Th} - (\alpha_p + \alpha_n)\omega^2)^2. \quad (9)$$

²The values measured in these experiments are *static* polarizabilities of the neutron, rather than the polarizabilities (often denoted $\bar{\alpha}$) we have been discussing here. In order to correct for this we have applied the standard 5% correction to obtain $\bar{\alpha}$'s from the experimental results [7].

The sum $\alpha_p + \alpha_n$ may then be accessible via its interference with the dominant Thomson term for the proton, f_{Th} [11]. This is one example of a general argument that the deuteron differential cross section is sensitive to isoscalar combinations of the nucleon polarizabilities. This means that with experimental knowledge of the proton polarizabilities it may be possible to extract those for the neutron. Coherent Compton scattering on a deuteron target has been measured at $E_\gamma = 49$ and 69 MeV by the Illinois group [12]. An experiment with tagged photons in the energy range $E_\gamma = 84.2 - 104.5$ MeV is under analysis at Saskatoon [13], while data for E_γ of about 60 MeV is being analyzed at Lund [14].

There is clearly a need for a consistent theoretical framework in order to interpret this data. The amplitude for Compton scattering on the deuteron involves mechanisms other than Compton scattering on the individual constituent nucleons. Hence, extraction of nucleon polarizabilities requires a theoretical calculation of Compton scattering on the deuteron that is under control in the sense that it accounts for *all* mechanisms to a given order in a systematic expansion in a small parameter. There exist a few calculations of this reaction in the framework of conventional potential models [15, 16, 7]. These calculations yield similar results if similar input is supplied, but typically mechanisms for nucleon polarizabilities and two-nucleon contributions are not treated consistently. We will see that χPT provides an alternative framework where this drawback can be eliminated.

In few-nucleon systems, a complication arises in χPT due to the existence of shallow nuclear bound states and related infrared singularities in A -nucleon reducible Feynman diagrams evaluated in the static approximation [17]. Physically, the fundamental problem is that nuclear physics introduces a new mass scale, the nuclear binding energy, which is very small compared to a typical hadronic scale. One way to overcome this difficulty is to adopt a modified power counting scheme in which χPT is used to calculate an effective potential which generally consists of all A -nucleon irreducible graphs. The S -matrix, which includes all reducible graphs as well, is then obtained through iteration by solving a Lippmann-Schwinger equation [17]. (We will refer to this version of the effective theory as the Weinberg formulation.) To date the Weinberg formulation can be carried through rigorously only using finite cutoff regularization [18, 19, 20, 21]. This limitation has spawned an intense theoretical effort geared at formulating an effective field theory for low-lying bound states which is verifiably (analytically) consistent in the sense of renormalization [22]. One result of this effort is a new power counting scheme in which all nonperturbative physics responsible for the presence of low-lying bound states arises from the iteration of a single operator in the effective theory, while all other effects, including all higher dimensional operators *and* pion exchange, are treated perturbatively [23, 24]. (We will refer to this version of the effective theory as the Kaplan-Savage-Wise (KSW) formulation.) This is relevant here because Compton scattering on the deuteron has been computed to next-to-leading order in the KSW formulation [25]. We will discuss this result and its relation to our calculation. A comprehensive and up-to-date review of nuclear applications of effective field theories can be found in Ref. [26].

In this paper we compute Compton scattering on the deuteron for incoming photon energies of order 100 MeV in the Weinberg formulation. We use baryon χPT to compute an irreducible scattering kernel to order Q^3 , which is then sewn to external deuteron wavefunctions as in Fig. 1. Compton scattering on the nucleon is a fundamental ingredient of our calculation. This is a direct consequence of the power counting scheme specific to the Weinberg formulation. It is important to realize that typical nucleon momenta inside the deuteron are small—on the order of \sqrt{MB} or m_π , with B the deuteron binding energy—and consequently, *a priori* we expect no convergence problems in the χPT expansion of any low-momentum electromagnetic or pionic probe of the deuteron. This method has led to fruitful computation of the pion-deuteron scattering length [17, 27], neutral pion photoproduction on the deuteron at threshold [28], as well as pn radiative capture [29] and the solar burning process $pp \rightarrow de^+\nu$ [30]. Although in principle we could use wavefunctions computed in χPT , we will consider wavefunctions generated using two modern nucleon-nucleon potentials. In previous computations using this method results are not very sensitive to details of the deuteron wavefunction. Any wavefunction with the correct binding energy gives equivalent results to within the theoretical error expected from neglected higher orders in the chiral expansion. Similar wavefunction independence is found here.

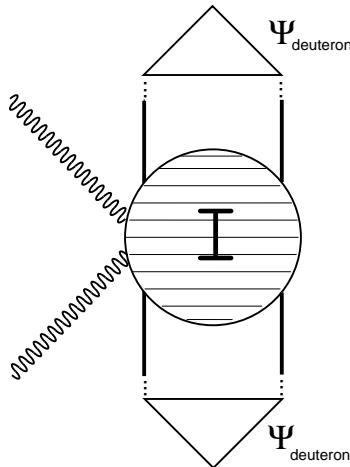


Figure 1: The anatomy of the calculation. The irreducible kernel (I) is computed in baryon χPT and sewn to external deuteron wavefunctions to give the matrix element for Compton scattering on the deuteron.

In Section 2 we review those aspects of χPT that are directly relevant to our calculation, including the power counting scheme and the relevant operators. In Section 3 we present the power counting for Compton scattering on the NN system. We discuss subtleties which arise because of the presence of a new mass scale in the two-nucleon system:

the deuteron binding energy. Then, in Section 4 we present our calculation of Compton scattering on the NN system to order Q^3 in baryon χPT . We discuss Compton scattering on a single nucleon—which has been calculated elsewhere [1, 2, 3]—and compute the Feynman amplitudes which contribute to photon scattering on the two-nucleon system at order Q^3 in the momentum expansion. In Section 5 we present results for differential cross sections for Compton scattering on unpolarized deuteron targets. We discuss higher-order effects and the extent to which a determination of neutron polarizabilities is possible. Finally, in Section 6 we summarize our work, and identify future directions for the theoretical study of this reaction.

2 Baryon Chiral Perturbation Theory

In this section, we briefly discuss the effective chiral Lagrangian underlying our calculations and the corresponding power counting. Precise statements about QCD dynamics at low energies can be made only where a small dimensionless expansion parameter is identified. This is of course the motivation behind the ongoing intense effort to develop a perturbative theory of nuclear interactions [26]. One class of dimensionless parameters consists of pure numbers, such as a coupling constant associated with a renormalizable interaction, or the inverse of the dimensionality of a group, as in the large- N_c expansion in QCD. A second class of dimensionless parameters consists of ratios of dimensional quantities which are present in a physical system when there is a clean hierarchy of scales. Effective field theory is the technology which develops a hierarchy of scales into a perturbative expansion of physical observables. In a system with broken symmetries this technology is especially powerful. When a continuous symmetry is spontaneously broken there are always massless Goldstone modes which dominate the low-energy dynamics. Although the symmetry in question is no longer a symmetry of the vacuum, it remains a symmetry of the Lagrangian. Moreover, massless Goldstone modes only couple derivatively. Hence at energies small relative to the characteristic symmetry breaking scale, the interactions of the Goldstone bosons can be ordered in an effective Lagrangian which is constrained by chiral symmetry and in which each operator contains a nonvanishing number of derivatives acting on the pion fields. Observables computed from the effective Lagrangian are therefore power series in momenta, with the non-analyticities required by perturbative unitarity.

In QCD the chiral $SU(2)_L \times SU(2)_R$ symmetry is spontaneously broken and the low-energy effective field theory is χPT . Here we are interested in processes where the typical momenta of all external particles is $p \ll \Lambda_\chi$, so we identify our expansion parameter as p/Λ_χ . If the chiral symmetry of QCD were exact this would be the only expansion parameter in χPT . However, in QCD $SU(2)_L \times SU(2)_R$ is softly broken by the small quark masses. This explicit breaking implies that the pion has a small mass in the low-energy theory. Since m_π/Λ_χ is then also a small parameter, we have a dual expansion in

p/Λ_χ and m_π/Λ_χ . We take Q to represent either a small momentum *or* a pion mass. A generic contribution to a matrix element involving the interaction of any number of pions and A nucleons can then be written in the form

$$\mathcal{M} = Q^\nu \mathcal{F}(Q/\mu), \quad (10)$$

where μ is a renormalization scale, $\mathcal{F}(x)$ is some non-analytic function, which is assumed to obey $\mathcal{F}(1) = O(1)$, and ν is a counting index. In general the full \mathcal{M} is the sum of a set of Feynman diagrams in a quantum field theory. It is straightforward to arrive at a general formula for ν by considering the momentum-space structure of generic Feynman rules [17].

First, we consider only irreducible subdiagrams. These are graphs in which the energies flowing through all internal lines are of $O(Q)$. The issue of calculating the full matrix element for the process of interest from this kernel will be taken up shortly. In irreducible diagrams we have the following counting rules:

- A nucleon propagator contributes Q^{-1} ;
- A pion propagator contributes Q^{-2} ;
- Each derivative or power of the pion mass at a vertex contributes Q ;
- Each loop integral contributes Q^4 ;
- Each delta function of four-momentum conservation contributes Q^{-4} .

In this way, we find that a diagram with A nucleons, L loops, C separately connected pieces, and V_i vertices of type i gives [17, 31]

$$\nu = 4 - A - 2C + 2L + \sum_i V_i \Delta_i, \quad (11)$$

where the so-called index of the interaction i is

$$\Delta_i \equiv d_i + f_i/2 - 2 \quad (12)$$

with d_i the sum of the number of derivatives or powers of m_π and f_i the number of nucleon fields.

Since pions couple to each other and to nucleons through either derivative interactions or quark masses, there is a lower bound on the index of the interaction: $\Delta_i \geq 0$. Hence the leading *irreducible* graphs are tree graphs ($L = 0$) with the maximum number of separately connected pieces ($C = \max$), and with vertices with $\Delta_i = 0$. Higher-order graphs (with larger powers of ν) are perturbative corrections to this leading effect. In this way, a perturbative series is generated by increasing the number of loops L , decreasing

the number of connected pieces C , and increasing the number of derivatives, pion masses and/or nucleon fields in interactions.

How is this analysis altered in the presence of an electromagnetic field? Photons couple via the electromagnetic field strength tensor and by minimal substitution. This has the simple effect of replacing a derivative by a factor of the charge e . This introduces a second expansion, in the small electromagnetic coupling $\alpha_{\text{em}} = e^2/4\pi$. Since we will be working at a fixed order in the expansion in α_{em} (leading order), it is convenient to enlarge the definition of d_i to include powers of e as well, thus continuing to classify interactions according to the index Δ_i defined by (12).

With the power counting scheme established, the next step is to construct the effective Lagrangians labelled by the interaction index Δ_i . The technology that goes into building an effective Lagrangian and extracting the Feynman rules is standard by now and presented in great detail in [1].

The pion triplet is contained in a matrix field

$$\Sigma = \xi^2 \equiv \sqrt{1 - \frac{\vec{\pi}^2}{f_\pi^2}} + i \frac{\vec{\pi} \cdot \vec{\tau}}{f_\pi}, \quad (13)$$

where $f_\pi = 93$ MeV is the pion decay constant. Under $SU(2)_L \times SU(2)_R$, Σ transforms as $\Sigma \rightarrow L\Sigma R^\dagger$ and ξ as $\xi \rightarrow L\xi U^\dagger = U\xi R^\dagger$; here $L(R)$ is an element of $SU(2)_L$ ($SU(2)_R$), and U is defined implicitly. It is convenient to assign the nucleon doublet N the transformation property $N \rightarrow UN$.

With $Q = (1 + \tau_3)/2$ we can write the pion covariant derivative as

$$D_\mu \Sigma = \partial_\mu \Sigma - ie\mathcal{A}_\mu [Q, \Sigma]. \quad (14)$$

Out of ξ one can construct

$$V_\mu = \frac{1}{2} [\xi^\dagger (\partial_\mu - ie\mathcal{A}_\mu Q) \xi + \xi (\partial_\mu - ie\mathcal{A}_\mu Q) \xi^\dagger] \quad (15)$$

$$A_\mu = \frac{i}{2} [\xi^\dagger (\partial_\mu - ie\mathcal{A}_\mu Q) \xi - \xi (\partial_\mu - ie\mathcal{A}_\mu Q) \xi^\dagger], \quad (16)$$

which transform as $V_\mu \rightarrow UV_\mu U^\dagger + U\partial_\mu U^\dagger$ and $A_\mu \rightarrow UA_\mu U^\dagger$ under $SU(2)_L \times SU(2)_R$. V_μ is used to build covariant derivatives of the nucleon,

$$D_\mu N = (\partial_\mu + V_\mu)N. \quad (17)$$

The electromagnetic field enters not only through minimal coupling in the covariant derivatives, but also through

$$f_{\mu\nu} = e(\xi^\dagger Q \xi + \xi Q \xi^\dagger) F_{\mu\nu}, \quad (18)$$

where $F_{\mu\nu}$ is the usual electromagnetic field strength tensor.

Because the nucleon mass is large, $M \gg Q$, it plays no dynamical role: nucleons are non-relativistic objects in the processes we are interested in. The field N can be treated as a heavy field of velocity v in which on-mass-shell propagation through $\exp(iMv \cdot x)$ has been factored out. In the rest frame of the nucleon, the velocity vector $v^\mu = (1, \vec{0})$. The spin operator is denoted by S^μ , and in the nucleon rest frame $S^\mu = (1/2)(0, \vec{\sigma})$.

With these ingredients, it is straightforward to construct the effective Lagrangian, conveniently ordered according to the index Δ_i of Eq. (12),

$$\mathcal{L} = \sum_{\Delta=0}^{\infty} \mathcal{L}^{(\Delta)}. \quad (19)$$

The leading-order Lagrangian is

$$\begin{aligned} \mathcal{L}^{(0)} = & \frac{1}{4}f_\pi^2 \text{tr}(D_\mu \Sigma^\dagger D^\mu \Sigma) + \frac{1}{4}f_\pi^2 m_\pi^2 \text{tr}(\Sigma + \Sigma^\dagger) \\ & + iN^\dagger(v \cdot D)N + 2g_A N^\dagger(A \cdot S)N \\ & - \frac{1}{2}C_a(N^\dagger \Gamma_a N)^2 \end{aligned} \quad (20)$$

where Γ_a is an arbitrary (non-derivative) Hermitian operator, and $g_A = 1.26$ and C_a are parameters. The sub-leading terms are contained in

$$\begin{aligned} \mathcal{L}^{(1)} = & \frac{1}{2M}N^\dagger(-D^2 + (v \cdot D)^2 + 2ig_A\{v \cdot A, S \cdot D\} \\ & - \frac{i}{2}[S^\mu, S^\nu][(1 + \kappa_v)f_{\mu\nu} + \frac{1}{2}(\kappa_s - \kappa_v)\text{tr}f_{\mu\nu}])N + \dots, \end{aligned} \quad (21)$$

where $\kappa_v = \kappa_p - \kappa_n$ and $\kappa_s = \kappa_p + \kappa_n$ are parameters related to the anomalous magnetic moments of the proton, $\kappa_p = 1.79$, and neutron, $\kappa_n = -1.91$. In sub-subleading order,

$$\mathcal{L}^{(2)} = -\frac{e^2}{32\pi^2 f_\pi} \pi_3 \epsilon^{\mu\nu\rho\sigma} F_{\mu\nu} F_{\rho\sigma} + \frac{e^2}{4M^2} \mathcal{Z}(\mathcal{Z} + 2\kappa)N^\dagger \vec{\sigma} \cdot (\vec{A} \times \vec{E})N + \dots \quad (22)$$

where the first term is from the anomaly, with $\epsilon_{0123} = 1$, and the second term is a $1/M^2$ correction expressed in the nucleon rest frame with electric field $\vec{E} = \partial_0 \vec{A}$ [2]. In our notation, $\kappa = \kappa_p$ when $\mathcal{Z} = 1$ and $\kappa = \kappa_n$ when $\mathcal{Z} = 0$ and in the expressions above, the ellipses signify that we have included only the interactions which are relevant to our calculation. Likewise, terms in $\mathcal{L}^{(n \geq 3)}$ do not appear in Compton scattering to the order that we are working.

Note, finally, that the Δ isobar can be introduced in a manner analogous to the nucleon field. The delta-nucleon mass difference $M_\Delta - M$ is not much larger than our Q , so integrating out the delta may worsen the convergence of the low-energy expansion considerably. Of course, the effects of the delta still appear in the effective theory constructed above, via their inclusion in counterterms, but keeping an explicit delta shifts these effects to lower orders in the expansion. For simplicity, in this initial calculation we do not include the delta.

3 Compton Counting

3.1 The role of nuclear physics

The power counting of chiral perturbation theory summarized above works very well for processes involving one or zero nucleons. A non-trivial new element enters the effective theory when we consider systems of more than one nucleon [17, 26]. Because nucleons are heavy, contributions from intermediate states that differ from the initial state only in the kinetic energy of nucleons are enhanced by infrared quasi-divergences. This is linked to the existence of small energy denominators $\sim Q^2/M$, which generate contributions $O(\Lambda_\chi/Q)$ larger than would be expected from Eq. (11). However, this is not really either a surprise or a problem. Eq. (11) was derived by assuming that all nucleon propagators scale as $1/Q$. This is correct for irreducible subdiagrams, which do not contain intermediate states with small energy denominators. In an A -nucleon system which is not subject to any external probes these diagrams are A -nucleon irreducible diagrams, the sum of which we call the potential V . (See e.g. the left-hand graph of Fig. 2.) To obtain the full two-nucleon Green's function these irreducible graphs are iterated using the free two-nucleon Green's function, which can, of course, have a small energy denominator which does not obey the χPT power-counting. This iteration gives contributions to the two-nucleon Green's function such as the graph shown on the right-hand side of Fig. 2. When we consider external probes with momenta of order Q , the sum of irreducible diagrams forms a kernel K for the process of interest. The full Green's function for the reaction is then found by multiplying this kernel K by two-particle Green's functions in which the two-particle propagators with small energy denominators may appear.

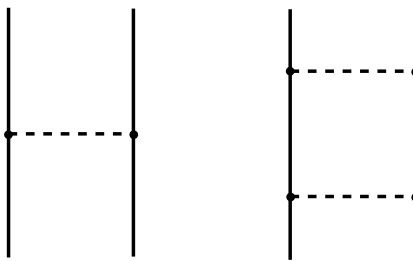


Figure 2: One- and two-pion exchange graphs. One-pion exchange is in the potential and (uncorrelated) two-pion exchange is generated by solving the Schrödinger equation.

In the case of Compton scattering on the two-nucleon system the formal version of these statements is as follows. The two-particle Green's function, G , is constructed from the two-nucleon-irreducible interaction V , and the free two-nucleon Green's function G_0 , via

$$G = G_0 + G_0VG. \quad (23)$$

Since V is two-particle irreducible we may perform a chiral power counting on it as per Eq. (11). Such a potential has been constructed up to $\nu = 3$, in Refs. [18, 19]. That work employed cutoff regularization, and the Schrödinger equation was solved to obtain the NN wave function. Fits to deuteron properties and scattering data up to laboratory energies of 100 MeV were obtained for three different cutoff parameters [20]. However, the quality of the fit is not as good as that of phenomenological models. Full consistency can be achieved by treating both the kernel for the interaction with external probes and the NN potential in the same framework. However, here we will follow a hybrid approach: we will calculate the kernel in χPT but use several “realistic” potential models to calculate the two-particle Green’s function.

To calculate Compton scattering on the two-nucleon system we must also identify the two-nucleon irreducible kernel, $K_{\gamma\gamma}$, for the process $\gamma NN \rightarrow \gamma NN$. Again, the power-counting of Eq. (11) applies to this object, since all nucleon denominators in it are, by definition, of $O(Q)$, as long as $\omega \sim Q$. The full Green’s function for Compton scattering on the two-nucleon system is then

$$G_{\gamma\gamma} = GK_{\gamma\gamma}G. \quad (24)$$

It follows that if $K_{\gamma\gamma}$ is constructed in a gauge invariant way and is worked out to the same order in χPT as the potential V then this calculation will be gauge invariant up to that order in chiral perturbation theory. However, even if $K_{\gamma\gamma}$ and V are consistently constructed this calculation is not *exactly* gauge invariant, since a brief examination of the counting explained above shows that contributions to $K_{\gamma\gamma}$ of the form

$$K_\gamma GK_\gamma, \quad (25)$$

where K_γ is the two-nucleon-irreducible kernel for one photon interacting with the two-nucleon system, only appear order-by-order in the expansion in Q/Λ_χ . In fact, for gauge invariance to be *exact* the contribution (25) must be included in full in $G_{\gamma\gamma}$.

Indeed, at low photon energies the contribution (25), known as the resonance contribution to Compton scattering, is crucial to a correct understanding of the reaction. In particular, without it the Thomson limit amplitude for Compton scattering on the deuteron will not be recovered. In this low-energy region the power-counting of Eq. (11) does not apply to $K_{\gamma\gamma}$, since graphs in $K_{\gamma\gamma}$ with two-nucleon intermediate states (Eq. (25)) can lead to violations of the power-counting via the same infrared quasi-divergences discussed above. However, if the energy of the probe is larger ($\sim m_\pi$) it is valid to look at the contributions $K_\gamma GK_\gamma$ using the power-counting of Eq. (11). Hence at higher photon energies it is completely correct to treat this resonance contribution only perturbatively in the Q expansion. In other words, as we move into the energy region which is well

above the poles of the Green's function G , it becomes reasonable to use a perturbative expansion for G in Eq. (25), rather than one which retains its full structure.

Arguments such as these lead us to identify two regimes for Compton scattering on nuclei, depending on the relation of the energy of the photonic probe, ω , to the typical nuclear binding scale $B \sim m_\pi^2/M$:

1. $\omega \sim B$. In this region the power-counting of Eq. (11) is not valid, since the external probe momentum flowing through the nucleon lines is of order Q^2/M , rather than order Q . It is in this region that the Compton low-energy theorems are derived. Therefore our power counting will not recover those low-energy theorems.
2. $\omega \sim Q \gg B$. In this region the power counting of Eq. (11) is valid, since in all irreducible graphs a photon energy of order Q flows through the nucleon lines.

These two regimes were identified by Friar and Tomusiak in a discussion of the role of low-energy theorems for threshold pion photoproduction on nuclei [32]. They were also discussed in the work of Chen *et al.* [25]. In Ref. [25] Compton scattering on the deuteron was computed to the same order discussed here, one order beyond leading non-vanishing order. However, there the calculation was performed in the KSW formulation of two-nucleon effective field theory, rather than in the Weinberg formulation. An advantage of KSW power-counting is that the effective field theory moves smoothly between $Q < B$ and $Q > B$. KSW power-counting is valid for nucleon momenta $Q < \Lambda_{NN} \sim 300$ MeV. Thus in the KSW formulation deuteron polarizabilities and Compton scattering up to energies $\omega < \Lambda_{NN}^2/M \sim 90$ MeV can be discussed in the same framework. Here we are interested mostly in the region $\omega \sim m_\pi$, and so we regard ourselves as being firmly in the second regime —although we shall see that this requires us to be cautious in our conclusions for Compton scattering at lower energies. In Fig. 3 we illustrate the ranges of validity of the KSW and Weinberg formulations of effective field theory of Compton scattering on the deuteron.

3.2 Power counting for $\gamma NN \rightarrow \gamma NN$

Let us now consider in more detail the kernel in the regime $\omega \sim m_\pi$. By definition, it consists of those irreducible subdiagrams to which the external photons are attached. One cannot cut these diagrams in two pieces without cutting at least one line with energy $O(Q)$. In particular, there are no irreducible graphs where the two photons are attached to different nucleons unless the two nucleons are connected by some interaction: energy and momentum conservation require the exchange of a pion or a short-range interaction to carry the energy $O(Q)$ from one nucleon to the other, and somewhere along the nucleon lines there is an energy flow of the order of the pion mass.

We will concentrate here on real Compton scattering on an $A = 2$ system and work in the Coulomb gauge where the incoming and outgoing photon momenta $k = (\omega, \vec{k})$ and $k' = (\omega', \vec{k}')$ and polarization vectors ϵ and ϵ' satisfy:

$$k^2 = 0; \quad k'^2 = 0; \quad v \cdot \epsilon = 0; \quad v \cdot \epsilon' = 0. \quad (26)$$

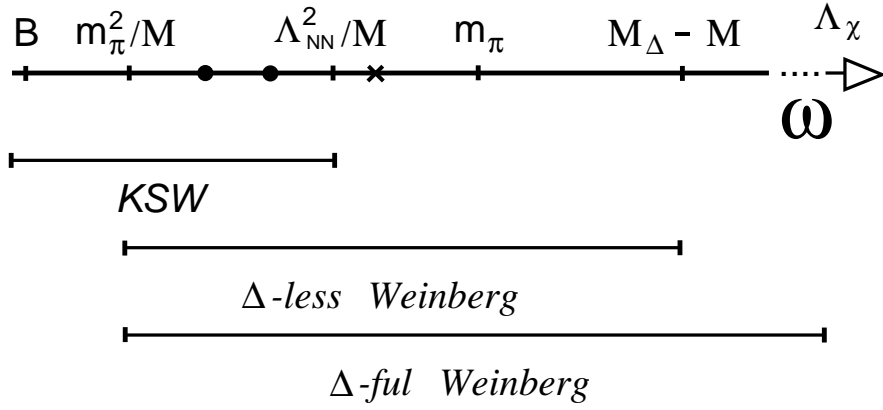


Figure 3: Hierarchy of scales and effective field theories of Compton scattering as a function of photon energy ω , as discussed in the text. The dots represent the experimental data from Illinois and the cross represents the forthcoming data from Saskatoon.

$$\underline{\nu = -2}$$

If we were interested in virtual photons, then the first contributions would start at $\nu = -2$. The leading effect would be from tree graphs ($L = 0$) with the maximum number of separately connected pieces ($C = 2$) constructed solely out of interactions with $\Delta_i = 0$ ($\sum_i V_i \Delta_i = 0$). The only possible graphs of this type come from the photon-nucleon interaction generated by minimal coupling in $\mathcal{L}^{(0)}$. For real photons these graphs vanish in the Coulomb gauge.

$$\underline{\nu = -1}$$

Likewise, some contributions at $\nu = -1$ are still tree graphs ($L = 0$) with the maximum number of separately connected pieces ($C = 2$), with one photon vertex of index one and one photon vertex of index zero ($\sum_i V_i \Delta_i = 1$). Graphs of this type do not contribute to real Compton scattering, if the Coulomb gauge is used. Similarly, all higher orders will include several diagrams that vanish for real photons in Coulomb gauge. From now on we do not discuss such graphs.

Thus, at this order the only contribution comes from a tree-level diagram with two separately connected pieces and a vertex which is the two-photon seagull of $\Delta_i = 1$. This vertex arises from minimal coupling in the kinetic nucleon terms in $\mathcal{L}^{(1)}$ of Eq. (21). It is depicted in Fig. 4(a).

$$\underline{\nu = 0}$$

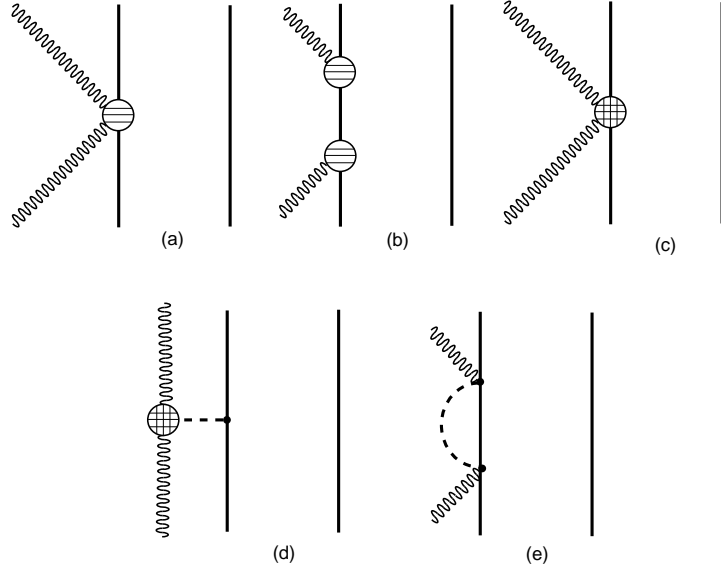


Figure 4: Characteristic one-body interactions which contribute to Compton scattering on the deuteron at order Q^2 (a) and at order Q^3 (b-e) (in the Coulomb gauge). Crossed graphs are not shown and not all loop topologies are shown. The sliced blobs are vertex insertions from $\mathcal{L}^{(1)}$. The sliced and diced blobs are vertex insertions from $\mathcal{L}^{(2)}$.

There are four types of corrections at this order:

1. Tree-level graphs ($L = 0$) with two separately connected pieces ($C = 2$) and two vertices with $\Delta_i = 1$ ($\sum_i V_i \Delta_i = 2$). Interactions with $\Delta_i = 1$ arise in $\mathcal{L}^{(1)}$ from minimal coupling in the kinetic nucleon term and from the Pauli terms associated with the anomalous magnetic moments. See Fig. 4(b).

Note that if these calculations are performed in the γNN center-of-mass frame then the boost of the γN interaction from the γN to the γNN c.m. frame appears naturally in the calculation. It occurs as a modification to these s and u -channel pole graphs which must be included because the total γN system three-momentum is non-zero.

2. Tree-level graphs ($L = 0$) with two separately connected pieces ($C = 2$) and one interaction with $\Delta_i = 2$ ($\sum_i V_i \Delta_i = 2$). Here a vertex in the $\mathcal{L}^{(2)}$ of Eq. (22) which is a relativistic correction to the magnetic interaction of the nucleon with the photons contributes. (See Fig. 4(c).) There is also a process involving exchange of a π^0 with the $\pi^0 \gamma \gamma$ interaction coming from the anomaly term in $\mathcal{L}^{(2)}$. (See Fig. 4(d).)
3. One-loop graphs ($L = 1$) with two separately connected pieces ($C = 2$) and all interactions from the $\mathcal{L}^{(0)}$ of Eq. (20) ($\sum_i V_i \Delta_i = 0$). (See Fig. 4(e).)

4. Tree graphs ($L = 0$) with only one separately connected piece ($C = 1$) and all interactions from $\mathcal{L}^{(0)}$ (See Fig. 5.)

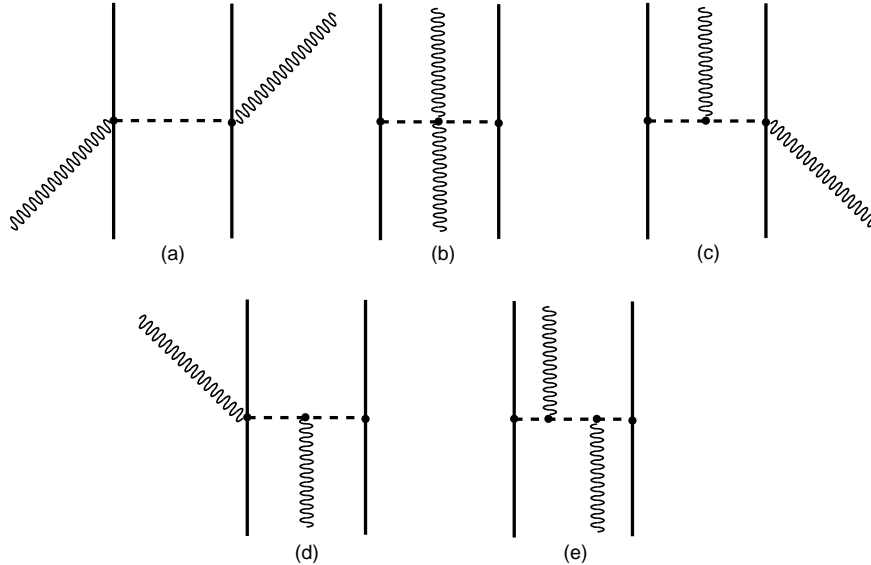


Figure 5: Two-body interactions which contribute to Compton scattering on the deuteron at order Q^3 . Permutations are not shown.

Note that we have not explicitly mentioned the delta anywhere in this discussion of our power counting. In the energy range of interest here, the delta could give important contributions. In fact, with the delta “integrated out”, as has been done here, its contributions first appear at $\nu = 1$, through counterterms. If the delta is included explicitly [33, 34], then it enters at order $\nu = 0$ via the loop graphs discussed under 3 above.

3.3 The breakdown of the power counting

The identification of the relevant contributions can be extended to higher orders in an obvious way. An example of a $\nu = 1$ (Q^4) contribution is shown in Fig. 6. We can use this graph to illustrate the transition to the very-low energy regime $Q \sim m_\pi^2/M$. It is easy to see that this graph becomes comparable to the order Q^3 graph of Fig. 5(a) when

$$\frac{|\vec{p}|^2}{\omega M} \sim 1. \quad (27)$$

Here \vec{p} is a typical nucleon momentum inside the deuteron and ω is the photon energy. Since our power counting is predicated on the assumption that all momenta are of order m_π , we find that our power-counting formula (11) is valid for the kernel $K_{\gamma\gamma}$ in the region

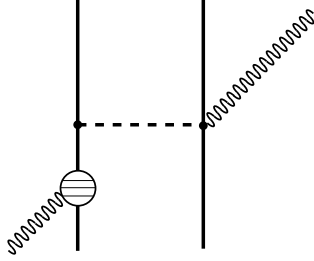


Figure 6: Two-body interaction which contributes to Compton scattering on the deuteron at order Q^4 . The sliced blob represents a $1/M$ correction vertex from $\mathcal{L}^{(1)}$.

$$\frac{m_\pi^2}{M} \ll Q \ll \Lambda_\chi. \quad (28)$$

In this first paper we will limit ourselves to a $\nu = 0$ (Q^3) calculation in the deltaless theory. We plan to study effects of an explicit delta field in a future publication. It is remarkable that to this order no unknown counterterms appear. All contributions to the kernel are fixed in terms of known pion and nucleon parameters such as m_π , g_A , M , and f_π . Thus, to this order χPT makes *predictions* for Compton scattering.

4 The χPT calculation

In this section, we outline how the various contributions are calculated. We can separate the contributions discussed in the previous section into two classes: one-nucleon and two-nucleon mechanisms. One-nucleon diagrams are those which relate directly to contributions to Compton scattering on a single nucleon, while two-nucleon mechanisms contribute only in $A \geq 2$ nuclei. One-nucleon scattering diagrams are traditionally labelled as Q^n with n the index in the one-nucleon process. We follow this usage here and above to make closer contact with the one-nucleon calculations. Of course only relative orders are physically significant.

4.1 One-nucleon contribution up to order Q^3 ($\nu \leq 0$)

Let us consider first the one-nucleon terms; a sample of the relevant diagrams is shown in Fig. 4. In the γN c.m. frame the nucleon amplitude can be written as

$$T_{\gamma N} = e^2 \left\{ A_1 \vec{\epsilon}' \cdot \vec{\epsilon} + A_2 \vec{\epsilon}' \cdot \vec{k} \vec{\epsilon} \cdot \vec{k}' + i A_3 \vec{\sigma} \cdot (\vec{\epsilon}' \times \vec{\epsilon}) + i A_4 \vec{\sigma} \cdot (\vec{k}' \times \vec{k}) \vec{\epsilon}' \cdot \vec{\epsilon} \right. \\ \left. + i A_5 \vec{\sigma} \cdot [(\vec{\epsilon}' \times \vec{k}) \vec{\epsilon} \cdot \vec{k}' - (\vec{\epsilon} \times \vec{k}') \vec{\epsilon}' \cdot \vec{k}] + i A_6 \vec{\sigma} \cdot [(\vec{\epsilon}' \times \vec{k}') \vec{\epsilon} \cdot \vec{k}' - (\vec{\epsilon} \times \vec{k}) \vec{\epsilon}' \cdot \vec{k}] \right\}. \quad (29)$$

The contribution at $\nu = -1$ ($O(Q^2)$) yields the low-energy theorem for Compton scattering from a single nucleon—the Thomson limit:

$$T_{\gamma N} = -\vec{\epsilon} \cdot \vec{\epsilon}' \frac{\mathcal{Z}^2 e^2}{M}, \quad (30)$$

where \mathcal{Z} is the nucleon charge. The tree graphs discussed under 1 and 2 for $\nu = 0$ in Section 3.2 have been known for a long time. The amplitude including these two sorts of contributions corresponds to a non-relativistic expansion of nucleon Born terms in a relativistic model with derivative coupling of the photon and Pauli magnetic moment interactions, plus a pion pole diagram. The differential cross section for scattering on the nucleon that results from these diagrams in the $g_A = 0$ limit is known as the Powell cross section. Adding diagrams of type 3 completes the $O(Q^3)$ amplitude in χPT without an explicit delta field [1, 2, 3].

Defining $\Upsilon = \omega/m_\pi$ and $t = -2\Upsilon^2(1 - \cos\theta)$, where θ is the center-of-mass angle between the incoming and outgoing photon momenta, one finds [1, 2, 3]:

$$\begin{aligned} A_1 &= -\frac{\mathcal{Z}^2}{M} + \frac{g_A^2 m_\pi}{8\pi f_\pi^2} \left\{ 1 - \sqrt{1 - \Upsilon^2} + \frac{2-t}{\sqrt{-t}} \left[\frac{1}{2} \arctan \frac{\sqrt{-t}}{2} - I_1(\Upsilon, t) \right] \right\}, \\ A_2 &= \frac{\mathcal{Z}^2}{M^2 \omega} - \frac{g_A^2}{8\pi f_\pi^2 m_\pi} \frac{2-t}{(-t)^{3/2}} [I_1(\Upsilon, t) - I_2(\Upsilon, t)], \\ A_3 &= \frac{\omega}{2M^2} [\mathcal{Z}(\mathcal{Z} + 2\kappa) - (\mathcal{Z} + \kappa)^2 \cos\theta] + \frac{(2\mathcal{Z} - 1)g_A m_\pi}{8\pi^2 f_\pi^2} \frac{\Upsilon t}{1-t} \\ &\quad + \frac{g_A^2 m_\pi}{8\pi^2 f_\pi^2} \left[\frac{1}{\Upsilon} \arcsin^2 \Upsilon - \Upsilon + 2\Upsilon^4 \sin^2 \theta I_3(\Upsilon, t) \right], \\ A_4 &= -\frac{(\mathcal{Z} + \kappa)^2}{2M^2 \omega} + \frac{g_A^2}{4\pi^2 f_\pi^2 m_\pi} I_4(\Upsilon, t), \\ A_5 &= \frac{(\mathcal{Z} + \kappa)^2}{2M^2 \omega} - \frac{(2\mathcal{Z} - 1)g_A}{8\pi^2 f_\pi^2 m_\pi} \frac{\Upsilon}{(1-t)} - \frac{g_A^2}{8\pi^2 f_\pi^2 m_\pi} [I_5(\Upsilon, t) - 2\Upsilon^2 \cos\theta I_3(\Upsilon, t)], \\ A_6 &= -\frac{\mathcal{Z}(\mathcal{Z} + \kappa)}{2M^2 \omega} + \frac{(2\mathcal{Z} - 1)g_A}{8\pi^2 f_\pi^2 m_\pi} \frac{\Upsilon}{(1-t)} + \frac{g_A^2}{8\pi^2 f_\pi^2 m_\pi} [I_5(\Upsilon, t) - 2\Upsilon^2 I_3(\Upsilon, t)], \end{aligned} \quad (31)$$

where

$$\begin{aligned} I_1(\Upsilon, t) &= \int_0^1 dz \arctan \frac{(1-z)\sqrt{-t}}{2\sqrt{1-\Upsilon^2 z^2}}, \\ I_2(\Upsilon, t) &= \int_0^1 dz \frac{2(1-z)\sqrt{-t(1-\Upsilon^2 z^2)}}{4(1-\Upsilon^2 z^2) - t(1-z)^2}, \\ I_3(\Upsilon, t) &= \int_0^1 dx \int_0^1 dz \frac{x(1-x)z(1-z)^3}{S^3} \left[\arcsin \frac{\Upsilon z}{R} + \frac{\Upsilon z S}{R^2} \right], \end{aligned}$$

$$\begin{aligned}
I_4(\Upsilon, t) &= \int_0^1 dx \int_0^1 dz \frac{z(1-z)}{S} \arcsin \frac{\Upsilon z}{R}, \\
I_5(\Upsilon, t) &= \int_0^1 dx \int_0^1 dz \frac{(1-z)^2}{S} \arcsin \frac{\Upsilon z}{R},
\end{aligned} \tag{32}$$

with

$$S = \sqrt{1 - \Upsilon^2 z^2 - t(1-z)^2 x(1-x)}, \quad R = \sqrt{1 - t(1-z)^2 x(1-x)}. \tag{33}$$

Because there is no counterterm consistent with chiral symmetry and gauge invariance at $O(Q^3)$, the sum of all loop graphs at this order is finite. Note that the loops contribute the same for protons and neutrons. Note also that, partly because of these loops, the Compton scattering amplitude is non-analytic in ω and in $\cos\theta$. For ω sufficiently small a power-series expansion in ω can be made. Up to an overall factor of α_{em} the coefficient of the term proportional to ω^2 in the invariant amplitude A_1 is then α_N , and that proportional to $\omega^2 \cos\theta$ is β_N . In this way we can extract the χPT predictions for the polarizabilities which were displayed in Eq. (3) [2]. These effects of the pion cloud dominate over short-range effects represented by higher-order contact terms. The lack of isospin dependence in loops then implies that in general the isoscalar polarizabilities are larger than the isovector ones. Furthermore, a numerical factor of 10 decreases the magnetic polarizabilities. Thus, in general we have, $\alpha_p \simeq \alpha_n \gg \beta_p \simeq \beta_n$. The agreement with the experimental values (4) and (5) is very good.

The difference between the full $O(Q^3)$ amplitude and the amplitude truncated at the level of the polarizabilities increases with energy. At $E_\gamma \sim 100$ MeV the typical error is 10%. However, the polarizability approximation favors forward directions, since at forward (backward) angles it overestimates (underestimates) the full amplitude. Two extreme cases are shown in Fig. 7. Both the full amplitude and the polarizability approximation are in relatively good agreement with data on the proton up to ~ 120 MeV [1, 35], although the agreement deteriorates with increasing energy and angle [35].

The only modification which must be made to the photon-nucleon amplitude (29) for use in Compton scattering on the deuteron is that it must be boosted from the γN c.m. frame to the γNN c.m. frame. To the order we are working this is easily accomplished, in one of two equivalent ways. Since only the s and u -channel nucleon-pole graphs depend on the nucleon momenta, these graphs can be computed in a frame in which the total γN three-momentum is non-zero (see Fig. 8), or the $O(Q^2)$ amplitude (30) can be boosted by making the appropriate substitutions to ensure that the polarization vectors $\vec{\epsilon}$ and $\vec{\epsilon}'$ stay orthogonal to \vec{k} and \vec{k}' in the new frame [36]. In both cases an additional term:

$$T_{\text{boost}} = -\frac{Z^2 e^2}{2M^2 \omega} [\vec{\epsilon} \cdot \vec{k}' \vec{\epsilon}' \cdot \vec{k} + 2(\vec{\epsilon} \cdot \vec{p} \vec{\epsilon}' \cdot \vec{k} + \vec{\epsilon} \cdot \vec{k}' \vec{\epsilon}' \cdot \vec{p})] \tag{34}$$

must be added to the one-body amplitude (29) when we are computing Compton scattering from the two-nucleon system at $O(Q^3)$.

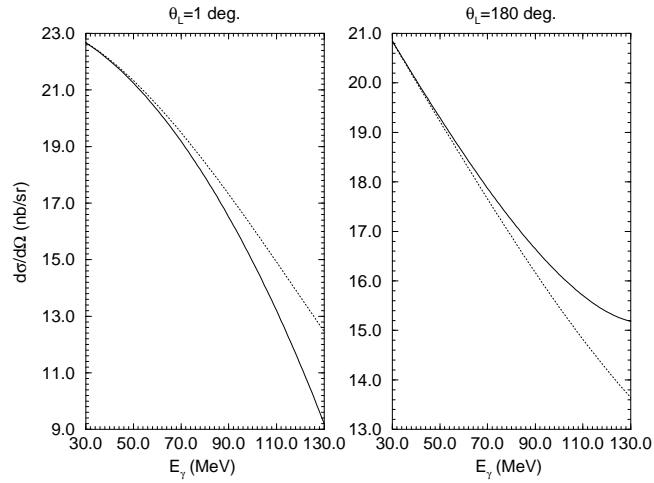


Figure 7: Unpolarized cross section for Compton scattering on the proton in deltaless χPT to $O(Q^3)$ as a function of the photon energy at two laboratory angles, $\theta_L = 1^\circ, 180^\circ$: polarizability approximation (dashed line) compared to full amplitude (solid line).

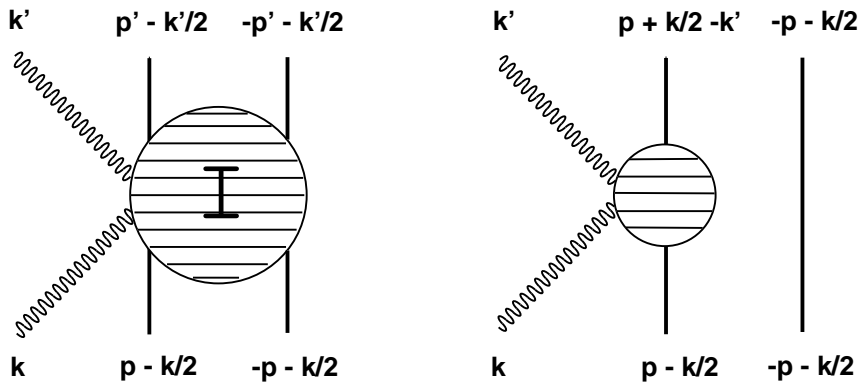


Figure 8: Labelling of 3-momenta for 2- and 1-nucleon mechanisms in the γNN c.m. frame.

As for higher-order mechanisms, effects of the $O(Q^4)$ terms in χPT on the nucleon polarizabilities have been studied. In Ref. [3] they were estimated to be considerable, especially in the case of the neutron magnetic polarizability:

$$\alpha_p = 10.5 \pm 2.0 \times 10^{-4} \text{ fm}^3; \quad \alpha_n = 13.4 \pm 1.5 \times 10^{-4} \text{ fm}^3; \quad (35)$$

$$\beta_p = 3.5 \pm 3.6 \times 10^{-4} \text{ fm}^3; \quad \beta_n = 7.8 \pm 3.6 \times 10^{-4} \text{ fm}^3. \quad (36)$$

Note that the uncertainties here are *theoretical* and arise from the use of resonance-saturation to estimate some of the $O(Q^4)$ χPT counterterms. The largest uncertainty concerns the effects of the delta isobar, which has a large electromagnetic transition to the nucleon via an M1 operator, and therefore affects β_N significantly. Consequently, the resonance-saturation estimate [3] of its tree-level contribution to a $\gamma\gamma NN$ counterterm is large, but in the case of β_p it is largely canceled by the $O(Q^4)$ πN loop contribution.

Attempts have been made to better determine the delta effects by inclusion of an explicit Δ field [33, 34]. This amounts to treating $M_\Delta - M$ as another quantity which is small relative to Λ_χ . The χPT expansion is then an expansion in the ratio of p , m_π and $M_\Delta - M$ to Λ_χ . These three small ratios are generically labelled ϵ . This ϵ expansion is certainly appropriate for the full amplitude at $p \sim m_\pi$, but possibly not very efficient for low-energy quantities such as the polarizabilities. The result of the explicit inclusion of the delta field is a shift of delta effects to lower orders. To $O(\epsilon^3)$ in this modified expansion there are large tree and loop contributions from delta graphs to β_N , but now there are no cancelations against πN graphs. There are also considerable loop contributions to α_N . The $O(\epsilon^3)$ result is [34]:

$$\alpha_p = \alpha_n = 16.4 \times 10^{-4} \text{ fm}^3; \quad (37)$$

$$\beta_p = \beta_n = 9.1 \times 10^{-4} \text{ fm}^3. \quad (38)$$

One can only hope that an $O(\epsilon^4)$ calculation will bring these values closer to the experimental ones of (4) and (5). Thus far, calculations to $O(Q^4)$ in the deltaless theory and to $O(\epsilon^3)$ in the deltaful theory have been limited to polarizabilities and to forward amplitudes, and so, as yet, in neither of these theories is there a calculation of the invariant functions A_1 – A_6 for arbitrary photon scattering angle.

4.2 Two-nucleon contributions at order Q^3 ($\nu = 0$)

The power counting discussed in Section 3 shows that when nuclear targets are involved a new contribution is present at the same order ($\nu = 0$) that the polarizabilities first appear: the two-nucleon contributions depicted in Fig. 5. In principle, then, we cannot hope to extract neutron polarizabilities without a theory for the two-nucleon contributions. Moreover, comparison of diagrams in Figs. 4(e) and 5 show that the same physics

that produces dominant contributions to the polarizabilities generates the dominant two-nucleon contributions. The only difference lies in the destination of the pion emitted by one nucleon: if it is absorbed on the same nucleon it contributes to the polarizability; if it lands on another nucleon, it generates a two-nucleon contribution. In this section we compute the dominant two-nucleon contributions in χPT —they involve no new parameters. It is also important to notice that these $O(Q^3)$ two-nucleon Feynman diagrams are the same as those at $O(\epsilon^3)$ in a theory in which the Δ is included explicitly. Only at next order would we find differences.

The two-nucleon amplitude from the diagrams in Fig. 5 is

$$T_{\gamma NN}^{2N} = -\frac{e^2 g_A^2}{2f_\pi^2} (\vec{\tau}^1 \cdot \vec{\tau}^2 - \tau_z^1 \tau_z^2) (t^{(a)} + t^{(b)} + t^{(c)} + t^{(d)} + t^{(e)}) \quad (39)$$

$$t^{(a)} = \frac{\vec{\epsilon} \cdot \vec{\sigma}^1 \vec{\epsilon}' \cdot \vec{\sigma}^2}{2[\omega^2 - m_\pi^2 - (\vec{p} - \vec{p}' + \frac{1}{2}(\vec{k} + \vec{k}'))^2]} + (1 \leftrightarrow 2) \quad (40)$$

$$t^{(b)} = \frac{\vec{\epsilon} \cdot \vec{\epsilon}' \vec{\sigma}^1 \cdot (\vec{p} - \vec{p}' - \frac{1}{2}(\vec{k} - \vec{k}')) \vec{\sigma}^2 \cdot (\vec{p} - \vec{p}' + \frac{1}{2}(\vec{k} - \vec{k}'))}{2[(\vec{p} - \vec{p}' - \frac{1}{2}(\vec{k} - \vec{k}'))^2 + m_\pi^2][(\vec{p} - \vec{p}' + \frac{1}{2}(\vec{k} - \vec{k}'))^2 + m_\pi^2]} + (1 \leftrightarrow 2) \quad (41)$$

$$t^{(c)} = -\frac{\vec{\epsilon}' \cdot (\vec{p} - \vec{p}' + \frac{1}{2}\vec{k}) \vec{\sigma}^1 \cdot \vec{\epsilon} \vec{\sigma}^2 \cdot (\vec{p} - \vec{p}' + \frac{1}{2}(\vec{k} - \vec{k}'))}{[\omega^2 - m_\pi^2 - (\vec{p} - \vec{p}' + \frac{1}{2}(\vec{k} + \vec{k}'))^2][(\vec{p} - \vec{p}' + \frac{1}{2}(\vec{k} - \vec{k}'))^2 + m_\pi^2]} + (1 \leftrightarrow 2) \quad (42)$$

$$t^{(d)} = -\frac{\vec{\epsilon} \cdot (\vec{p} - \vec{p}' + \frac{1}{2}\vec{k}') \vec{\sigma}^1 \cdot (\vec{p} - \vec{p}' - \frac{1}{2}(\vec{k} - \vec{k}')) \vec{\sigma}^2 \cdot \vec{\epsilon}'}{[\omega^2 - m_\pi^2 - (\vec{p} - \vec{p}' + \frac{1}{2}(\vec{k} + \vec{k}'))^2][(\vec{p} - \vec{p}' - \frac{1}{2}(\vec{k} - \vec{k}'))^2 + m_\pi^2]} + (1 \leftrightarrow 2) \quad (43)$$

$$t^{(e)} = \frac{2\vec{\epsilon} \cdot (\vec{p} - \vec{p}' + \frac{1}{2}\vec{k}') \vec{\epsilon}' \cdot (\vec{p} - \vec{p}' + \frac{1}{2}\vec{k}) \vec{\sigma}^1 \cdot (\vec{p} - \vec{p}' - \frac{1}{2}(\vec{k} - \vec{k}')) \vec{\sigma}^2 \cdot (\vec{p} - \vec{p}' + \frac{1}{2}(\vec{k} - \vec{k}'))}{[\omega^2 - M_\pi^2 - (\vec{p} - \vec{p}' + \frac{1}{2}(\vec{k} + \vec{k}'))^2][(\vec{p} - \vec{p}' - \frac{1}{2}(\vec{k} - \vec{k}'))^2 + m_\pi^2][(\vec{p} - \vec{p}' + \frac{1}{2}(\vec{k} - \vec{k}'))^2 + m_\pi^2]} + (1 \leftrightarrow 2) \quad (44)$$

We calculate the cross section for Compton scattering on the deuteron including the single-scattering and two-nucleon mechanisms described above. Our calculation represents therefore the full $\nu = 0$, or order Q^3 , χPT predictions for Compton scattering on the deuteron.

5 Results and discussion

To calculate the amplitude for Compton scattering on the deuteron we must take the residue of Eq. (24) at the initial and final bound-state pole. This leads to the amplitude

$$T^{\gamma d} = \langle \psi_d | K_{\gamma\gamma} | \psi_d \rangle, \quad (45)$$

where $|\psi_d\rangle$ is the deuteron wave function and we may eliminate the isospin factor by making use of the relation $\langle \psi_d | (\vec{\tau}^1 \cdot \vec{\tau}^2 - \tau_z^1 \tau_z^2) | \psi_d \rangle = -2$.

In Section 4 we wrote down both the one and two-body contributions to $K_{\gamma\gamma}$ at $O(Q^3)$ in the chiral expansion. If we make the same separation here then we can write down the following integrals for $T_{\gamma d}$ in the γd center-of-mass frame:

$$\begin{aligned}
T_{M'\lambda'M\lambda}^{\gamma d}(\vec{k}', \vec{k}) &= \int \frac{d^3p}{(2\pi)^3} \psi_{M'}\left(\vec{p} + \frac{\vec{k} - \vec{k}'}{2}\right) T_{\gamma N\lambda'\lambda}^{\gamma d \text{ c.m.}}(\vec{k}', \vec{k}) \psi_M(\vec{p}) \\
&+ \int \frac{d^3p d^3p'}{(2\pi)^6} \psi_{M'}(\vec{p}') T_{\gamma NN\lambda'\lambda}^{2N}(\vec{k}', \vec{k}) \psi_M(\vec{p})
\end{aligned} \tag{46}$$

where M (M') is the initial (final) deuteron spin state, and λ (λ') is the initial (final) photon polarization state, and \vec{k} (\vec{k}') the initial (final) photon three-momentum, which are constrained to $|\vec{k}| = |\vec{k}'| = \omega$. Note that the single-scattering γN T -matrix $T_{\gamma N}^{\gamma d \text{ c.m.}}$ must be evaluated in the γd center-of-mass frame. In χPT this is straightforward, as discussed in the previous section. Note also that all sums over the spins of the two nucleons have been suppressed here.

In general, for the wave function ψ we use the energy-independent Bonn OBEPQ wave function parameterization which is found in Ref. [37]. The photon-deuteron T -matrix (46) is then calculated and the laboratory differential cross section evaluated directly from it:

$$\frac{d\sigma}{d\Omega_L} = \frac{1}{16\pi^2} \left(\frac{E'_\gamma}{E_\gamma}\right)^2 \frac{1}{6} \sum_{M'\lambda'M\lambda} |T_{M'\lambda'M\lambda}^{\gamma d}|^2, \tag{47}$$

where E_γ is the initial photon energy in the laboratory frame, and is related to ω , the photon energy in the γd center-of-mass frame, via:

$$\omega = \frac{E_\gamma}{\sqrt{1 + 2E_\gamma/M_d}}; \tag{48}$$

and E'_γ is the final photon energy in the laboratory frame:

$$E'_\gamma = \frac{E_\gamma M_d}{M_d + E_\gamma(1 - \cos\theta_L)}. \tag{49}$$

Convergence tests indicate that with the numbers of quadratures chosen the cross section evaluated in this fashion is numerically accurate at about the 1% level. Of course, this error does not include the theoretical error from uncertainties due to different deuteron wave functions, and the effect of higher-order terms in the χPT calculation of the kernel. These errors will be discussed further below.

The rest of this section is divided into four subsections. First we display our results for this straightforward $O(Q^3)$ calculation. Results are presented at laboratory photon energies of 49, 69, and 95 MeV. At the lower two energies we compare with the experimental data of Lucas [12]. Data at $E_\gamma = 95$ MeV are expected soon from a recent

Saskatoon tagged photon Compton scattering experiment [13]. Second, we observe that at lower energies contributions due to NN states with relative momenta of order $\sqrt{M\omega}$ lead to certain diagrams being enhanced over the value expected from the power counting of Section 2. Indeed, as discussed in Section 3, we expect this power counting to break down for $\omega \sim m_\pi^2/M$. We estimate the effect of these contributions by calculating the impact some of them have on the differential cross section for photon-deuteron scattering. Third, we display the sensitivity of our results to the choice of deuteron wave function. Re-calculating our amplitudes with ψ_d defined by solving the Schrödinger equation with the Nijm93 potential [38] allows us to estimate the error associated with uncertainties in the NN interaction. Finally, in order to see the size of the effects we can expect in an $O(Q^4)$ calculation of this process, we arbitrarily include two terms which contribute to the $O(Q^4)$ calculation: counterterms which shift the values of the nucleon polarizabilities from the $O(Q^3)$ result.

5.1 Results at $O(Q^3)$

In figures 9, 10 and 11 below we display our results at 49, 69, and 95 MeV. For comparison we have included the calculation at $O(Q^2)$, where the second contribution in Eq. (46) is zero, and the γN T -matrix in the single-scattering contribution is given by the Thomson term on a single nucleon, Eq. (30).

The curves show that the correction from the $O(Q^3)$ terms gets larger as ω is increased, as was to be expected. Indeed, while at lower energies corrections are relatively small, in the 95 MeV results the correction to the differential cross section from the $O(Q^3)$ terms is of order 50%, although the contribution of these terms to the *amplitude* is of roughly the size one would expect from the power counting: about 25%. Nevertheless, it is clear, even from these results, that this calculation must be performed to $O(Q^4)$ before conclusions can be drawn about polarizabilities from data at photon energies of order m_π . This is in accord with similar convergence properties for the analogous calculation for threshold pion photoproduction on the deuteron [28].

We have also shown the six Illinois data points at 49 and 69 MeV [12]. Statistical and systematic errors have been added in quadrature. It is quite remarkable how well the $O(Q^2)$ calculation reproduces the 49 MeV data. However, it is clear that the agreement at forward angles is somewhat fortuitous, as there are significant $O(Q^3)$ corrections. Meanwhile, the agreement of the $O(Q^3)$ calculation with the 69 MeV data is very good, although only limited conclusions can be drawn, given that there are only two data points, each with sizeable error bars.

The energy-dependence of our results at a given angle is due to a combination of two mechanisms. First, at backward angles the $O(Q^2)$ deuteron Compton scattering amplitude

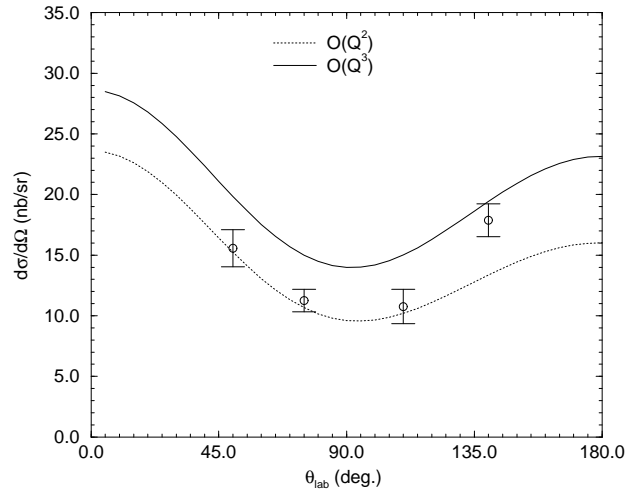


Figure 9: Results of the $O(Q^2)$ (dotted line) and $O(Q^3)$ (solid line) calculations at a photon laboratory energy of 49 MeV. The data points of Ref. [12] are also shown.

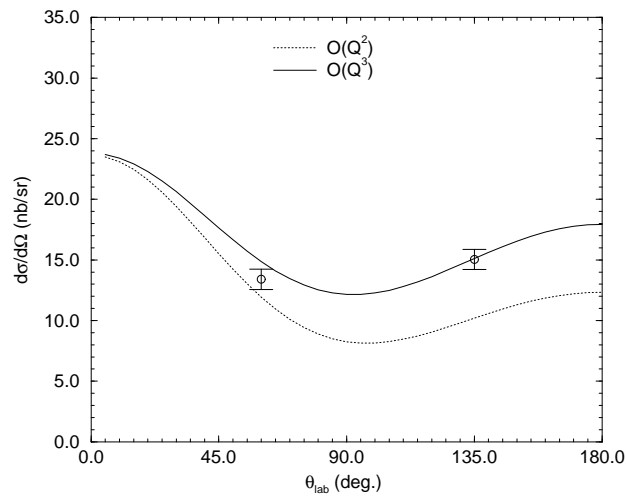


Figure 10: Results of the $O(Q^2)$ (dotted line) and $O(Q^3)$ (solid line) calculations at a photon laboratory energy of 69 MeV. The data points of Ref. [12] are also shown.

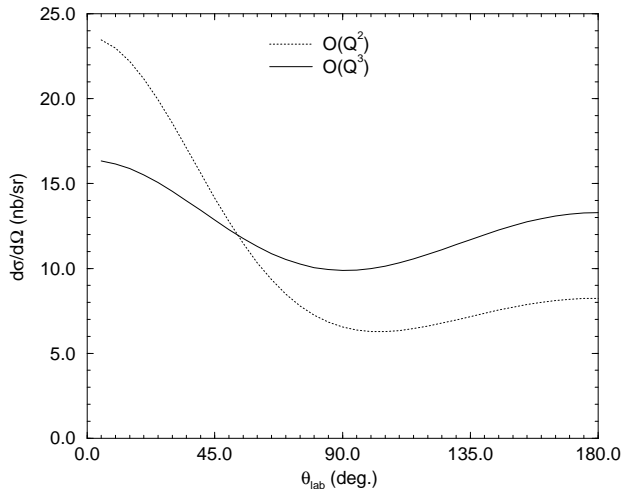


Figure 11: Results of the $O(Q^2)$ (dotted line) and $O(Q^3)$ (solid line) calculations at a photon laboratory energy of 95 MeV.

has energy-dependence, due to its proportionality to the non-relativistic deuteron charge form factor at a momentum transfer

$$\vec{q} = \vec{k} - \vec{k}'. \quad (50)$$

At forward angles this energy-dependence is minimal, since $|\vec{q}|^2$ is proportional to $\omega^2(1 - \cos\theta)$. Second, at both forward and backward angles the amplitude also has significant energy-dependence due to the structure of the single-nucleon amplitude (29) as a function of ω . This is particularly apparent at $\theta_{cm} = 0$, where the $O(Q^2)$ amplitude is, in fact, energy-independent, and we can see that the polarizabilities play a significant role in suppressing the forward differential cross section as the photon energy increases.

Our results are qualitatively not very different from other existing calculations. At 49 and 69 MeV our $O(Q^3)$ results are very close to those in Ref. [15] and a few nb/sr higher, especially at back angles, than those of Refs. [16, 7] (which are similar at these energies). At 95 MeV our $O(Q^3)$ result is close to that of Ref. [16], higher by several nb/sr at back angles than Ref. [7], and several nb/sr lower than the calculation with no polarizabilities of Ref. [15]³. Comparing to the calculations of deuteron Compton scattering in the KSW formulation of effective field theory [25], we see that the result of Ref. [25] is significantly lower than those presented here at both 49 and 69 MeV. At 49 MeV the

³At this energy Ref. [15] only presents results with $\alpha_p + \alpha_n = \beta_p + \beta_n = 0$, which in turn are considerably less forward peaked than the corresponding calculation of Ref. [16].

agreement of Ref. [25]’s calculation with the data is better than ours. We shall show in the next section that this is partly because 49 MeV is at the lower end of the domain of applicability of the Weinberg formulation. At 69 MeV our calculation does a slightly better job of reproducing the (two) data points available. The qualitative agreement among these calculations is a reflection of the similarities of mechanisms involved. Ours is however the only calculation to incorporate the full single-nucleon amplitude instead of its polarizability approximation. As shown in Figure 12 our tendency to higher cross sections in the backward directions is at least in part due to this feature, as expected from the discussion in Sect. 4.

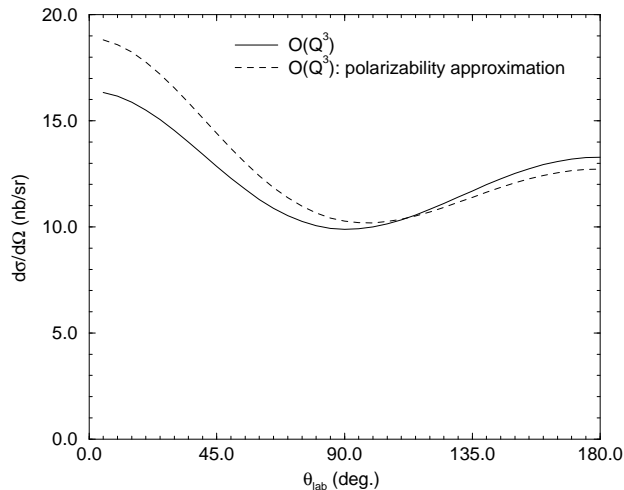


Figure 12: Unpolarized cross section for Compton scattering on the deuteron in deltaless χPT to $O(Q^3)$ at 95 MeV. The polarizability approximation to the single-nucleon amplitude (dashed line) is to be compared with the full $O(Q^3)$ calculation (solid line).

5.2 The breakdown of the power counting at low energies

In this section we examine the breakdown of the power counting defined by Eq. (11) at low energies. Recall that this power counting was only derived for photon energies of order m_π . Here we will calculate one portion of a particular diagram, and show how the contribution of that diagram becomes enhanced beyond the expectations of power counting if the photon energy becomes too low.

Consider the diagram shown in Figure 13. If the photon energy ω is of order m_π and therefore much larger than the nuclear binding and the nucleon kinetic energies then

the denominator of the intermediate-state NN propagator can be approximated by $1/\omega$. Effects due to the motion of bound nucleons then appear as higher-order vertices in the χPT Lagrangian, while effects due to binding also occur at higher order in the calculation. This is the approach adopted in this work. However, as ω is decreased, replacing the denominator in the two-nucleon propagator by ω is no longer a valid approximation. It becomes necessary to retain the full energy-dependence for dynamical nucleons, rather than use the heavy-baryon propagator which treats the nucleon as a static source. Thus, in this section we evaluate this graph using a propagator which retains the full momentum dependence for the two-nucleon intermediate state. In heavy-baryon chiral perturbation theory this means replacing the standard heavy baryon χPT propagator for two nucleons with energy ω by one in which a set of nominally higher-order corrections representing the motion of the nucleons has been resummed [17]:

$$\frac{1}{\omega} \longrightarrow \frac{M}{M\omega - \vec{p}^2}, \quad (51)$$

with \vec{p} the relative three-momentum of the two-nucleon state.

To simplify matters we consider only the vertices from the χPT Lagrangian $\mathcal{L}^{(1)}$ which arise from electric coupling of the photon to the nucleon. This gives:

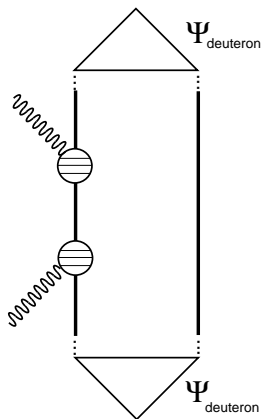


Figure 13: Contribution to Compton scattering on the deuteron from the s -channel pole in photon-nucleon scattering.

$$T_{s\text{-channel pole}} = \int \frac{d^3p}{(2\pi)^3} \psi \left(\vec{p} + \frac{\vec{k} - \vec{k}'}{2} \right) \frac{\vec{\epsilon}' \cdot (2\vec{p} + \vec{k} - \vec{k}')}{M} \frac{M}{M(\omega - B) - (\vec{p} + \frac{\vec{k}}{2})^2 + i\eta} \frac{\vec{\epsilon} \cdot (2\vec{p})}{M} \psi(\vec{p}) \quad (52)$$

To estimate the size of effects arising from the dynamical nature of the nucleons in the intermediate NN state we have rewritten the two-nucleon propagator as:

$$\frac{M}{M(\omega - B) - \left(\vec{p} + \frac{\vec{k}}{2}\right)^2 + i\eta} = P \frac{M}{M(\omega - B) - \left(\vec{p} + \frac{\vec{k}}{2}\right)^2} - iM\pi\delta\left(M\omega - MB - \left(\vec{p} + \frac{\vec{k}}{2}\right)^2\right). \quad (53)$$

For the case of low-energy photon-deuteron scattering the leading contribution to the delta-function piece will be $\delta(M\omega - \vec{p}^2)$. Thus, we may evaluate the leading part of the delta-function piece of $T_{s\text{-channel pole}}$ as a two-dimensional integral over the solid angle Ω_p :

$$T_{s\text{-channel pole}} = \frac{i\pi}{2\sqrt{M\omega}M} \int \frac{d^3p}{(2\pi)^3} \psi\left(\vec{p} + \frac{\vec{k} - \vec{k}'}{2}\right) 2\vec{\epsilon}' \cdot \vec{p} \delta(|\vec{p}| - \sqrt{M\omega}) 2\vec{\epsilon} \cdot \vec{p} \psi(\vec{p}). \quad (54)$$

Naively this expression contributes to $T^{\gamma d}$ at an order $\sqrt{\omega/\Lambda_\chi}$ relative to the leading contribution. However, note that in fact this part of $T_{s\text{-channel pole}}$ is suppressed beyond the level indicated by this straightforward counting, since factors of the deuteron wave function at momenta of order $\sqrt{M\omega}$ enter. Ultimately if $\omega \sim m_\pi$ these factors drastically reduce this piece of $T_{s\text{-channel pole}}$, rendering it quite small. However, at $\omega = 49$ MeV, contributions such as (54) can be sizeable⁴.

A contribution to Compton scattering on the deuteron similar to that of (54) exists for the u -channel pole graph for photon-nucleon scattering. The contribution of that graph to the amplitude is, in fact, real, and the loop momentum that contributes to that process is, at lowest order, $|\vec{p}| = i\sqrt{M\omega}$. In fact, as explained in Refs. [25] it is the contribution from these momenta in the u -channel pole graph that facilitates the (approximate) recovery of the Thomson limit for low-energy photon scattering off the deuteron.

When these two contributions are added to the amplitude $T^{\gamma d}$ calculated above we obtain the results shown in Figure 14. There we have shown results for $O(Q^2)$ and $O(Q^3)$, both with and without these mechanisms, at laboratory photon energies of 49, 69, and 95 MeV. Clearly the contribution from these two-nucleon states with relative momenta of order $\sqrt{M\omega}$ plays a significant role if $E_\gamma = 49$ MeV. Since these effects are higher-order in our power counting this apparently implies a breakdown of our approach at $\omega \sim 50$ MeV. However, we observe that once this NN intermediate-state contribution is added the agreement with the experimental data at 49 MeV is really quite good. This suggests that it may be possible to devise an alternative power counting for this regime, where an accounting is made not only of the way the scales ω , p and m_π appear in the amplitude, but also of the role played by the additional scale $\sqrt{M\omega}$.

⁴The role of such contributions from on-shell intermediate-state nucleons in neutral pion photoproduction on the deuteron was emphasized by Wilhelm [39]. In contrast to the case of photoproduction, in Compton scattering the incoming photon can be arbitrarily soft, so such contributions are unarguably important if the photon energy is low enough.

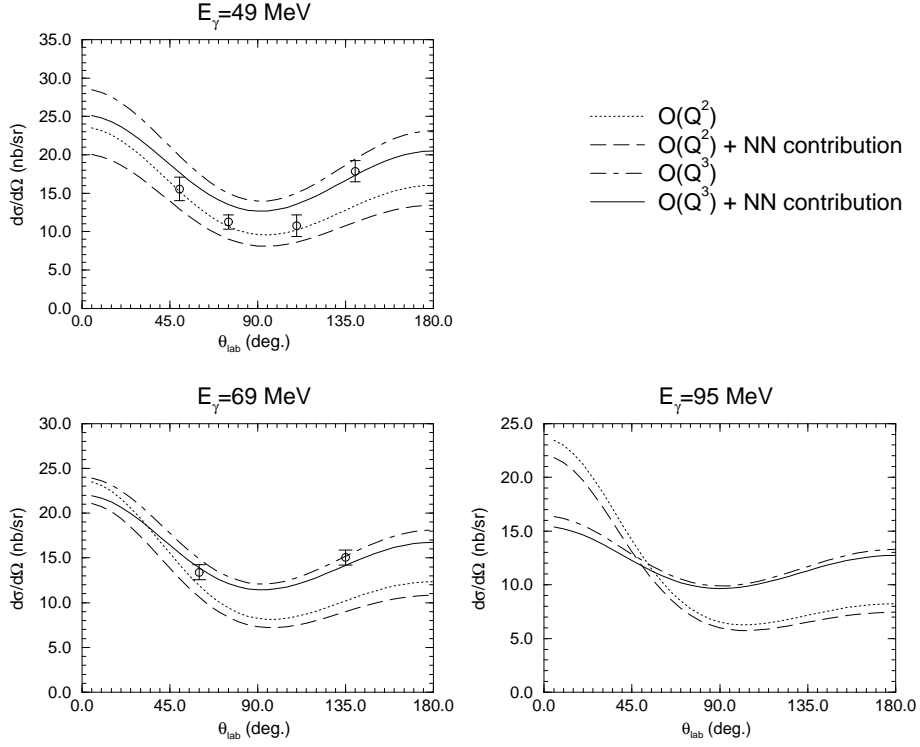


Figure 14: Results of calculations at 49, 69, and 95 MeV both with and without the contribution from NN intermediate states whose relative momenta are of order $\sqrt{M\omega}$. In each case the dotted line is the $O(Q^2)$ calculation, and the dot-dashed line is the $O(Q^3)$ calculation. Meanwhile the dashed line is an $O(Q^2)$ calculation with the contributions from NN intermediate-states with momenta of $O(\sqrt{M\omega})$ included, and the solid line is an $O(Q^3)$ calculation with the same contributions included. Experimental data from Ref. [12] are also shown.

However, this low-energy regime is not a primary concern in our work here. We have instead focused on $\omega \sim m_\pi$, since it is there that the best opportunity to extract the neutron polarizability seems to lie. Our results show that as the photon energy is increased the contribution from these on-shell NN intermediate states becomes significantly less, because of the suppression from the deuteron wave function discussed above. By the time $\omega = 95$ MeV is reached this higher-order effect is small: in fact, as we shall see below, it is significantly smaller than other higher-order effects which could be included.

5.3 Sensitivity to choice of deuteron wave function

We have also performed the calculation of the photon-deuteron differential cross section with a wave function found by solving the Schrödinger equation with the Nijm93 potential [38]. A comparison of $O(Q^3)$ calculations with the two different potentials at 49, 69, and 95 MeV is shown in Figure 15. The results with the Nijm93 wave function are in general a little higher than those found with OBEPQ. However, the cross sections only differ at the 10% level.

Further investigation shows that much of this discrepancy is due to inconsistency between the physics of pion range in the NN potentials employed and the two-nucleon Compton scattering mechanisms involving pions which we have calculated. In computing these graphs we employed the πNN vertex from the lowest-order chiral Lagrangian and the axial coupling constant $g_A = 1.26$. Therefore in essence we have used a πNN coupling in these graphs given by the Goldberger-Treiman relation:

$$f_{\pi NN}^2 \Big|_{\text{GT}} = \frac{g_A^2 m_\pi^2}{16\pi f_\pi^2} = 0.071. \quad (55)$$

In contrast, the values of f^2 employed in the two NN potentials from which we obtain our deuteron wave functions are:

$$f_{\pi NN}^2 \Big|_{\text{Bonn}} = 0.079; \quad f_{\pi NN}^2 \Big|_{\text{Nijm93}} = 0.075. \quad (56)$$

Effects beyond the leading-order result for $f_{\pi NN}$, Eq. (55), will enter at orders beyond those we have considered here and presumably move our $f_{\pi NN}$ towards the values (56). Although such changes in $f_{\pi NN}$ would be higher order in the chiral expansion, we note that in certain circumstances they may enter raised to the fourth power in the photon-deuteron cross section, and so might play a non-negligible role.

A fully consistent resolution of this issue must await the use of an accurate χ PT deuteron wave function in the calculation of deuteron Compton scattering. To address the issue in our current calculation we multiplied the strength of our two-nucleon mechanisms by two different factors in the calculations employing the two different deuteron wave functions. In this way the two-nucleon current is made consistent with the value of the

πNN coupling employed in the Nijm93 and OBEPQ potentials. We stress that the two potentials still do not have the same strength at pion range, but at least once such a scaling is employed the NN mechanisms for Compton scattering are always consistent with the one-pion exchange used to obtain the deuteron wave function. This partial remediation of the inconsistency reduced the wave function sensitivity to about 5% everywhere. This suggests to us that the difference between the results obtained with the two different wave functions does not represent a true sensitivity to short-distance dynamics, but rather a need to treat the dynamics of pion range in the same way in all pieces of the calculation.

As we shall see, this wave-function dependence is smaller than other effects which are higher-order in the chiral expansion of the kernel. Therefore at this stage we are not concerned about it. Ultimately we would like to perform this calculation of Compton scattering on the deuteron with a deuteron wave function calculated consistently from an NN potential derived within the χPT framework [20].

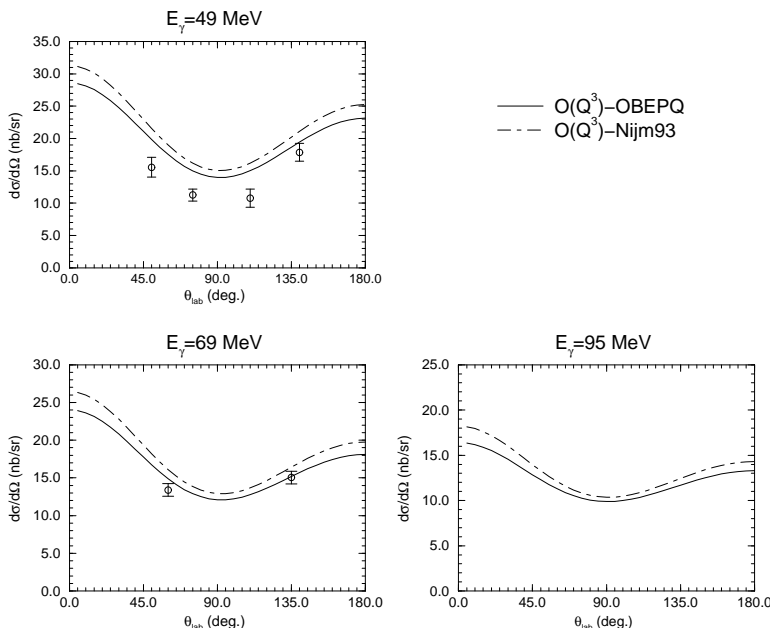


Figure 15: Results of calculations at 49, 69, and 95 MeV using two different NN wave functions in the $O(Q^3)$ calculation. The solid line is the result using the OBEPQ wave function, and the dot-dashed line using the Nijm93 wave function. Experimental data from Ref. [12] are also shown.

5.4 Effects of higher-order terms

Finally, in order to test the sensitivity of our calculation to higher-order effects we added a small piece of the $O(Q^4)$ amplitude for Compton scattering off a single nucleon. Specifically, we modified the invariant functions A_1 and A_2 of Eq. (31) to include additional terms. The additional terms are

$$\Delta A_1 = (\Delta\alpha + \Delta\beta \cos\theta) \omega^2, \quad (57)$$

$$\Delta A_2 = -\Delta\beta. \quad (58)$$

We emphasize that these are only two of a number of new terms which will appear in the single-nucleon scattering amplitude $T_{\gamma N}$ at $O(Q^4)$. Furthermore, a number of additional two-body mechanisms must be included in $T_{\gamma NN}^{2N}$ in any $O(Q^4)$ calculation of Compton scattering on the deuteron. Nevertheless, here we calculate the differential cross section with the terms (57) and (58) in order to get a feel for the sensitivity of our result to the presence of such higher-order terms.

The addition of (57) and (58) change the polarizabilities in the calculation to

$$\alpha = \alpha^{(Q^3)} + \Delta\alpha, \quad \beta = \beta^{(Q^3)} + \Delta\beta, \quad (59)$$

where $\alpha^{(Q^3)}$ and $\beta^{(Q^3)}$ are the $O(Q^3)$ values of Eq. (3).

Two calculations were performed. In the first, $\Delta\alpha$ and $\Delta\beta$ were chosen so that the total polarizabilities (59) were equal to the “experimental” values (4), (5), and (6). The second calculation involved a more dramatic change in the polarizabilities: $\Delta\alpha$ and $\Delta\beta$ were chosen so that α and β were equal to the $O(Q^4)$ values of Eqs. (35) and (36). In either case $\Delta\alpha_p + \Delta\alpha_n$ is relatively small, while $\Delta\beta_p + \Delta\beta_n$ is not large for “experimental” values, but is significant for the $O(Q^4)$ values. The results of these two calculations for the two photon energies $E_\gamma = 49$ MeV and $E_\gamma = 95$ MeV are shown in Fig. 16 and Fig. 17.

In both cases we see that, just as one would expect, the cross section at 95 MeV is much more sensitive to these $O(Q^4)$ terms than the cross section at 49 MeV. It is not surprising that the calculation with $O(Q^4)$ polarizabilities exhibits a larger change than that with “experimental” values. Continually increasing $\beta_p + \beta_n$ at approximately constant $\alpha_p + \alpha_n$ decreases the cross section at forward angles and increases it at back angles. In fact, it seems that if $\beta_p + \beta_n$ is sufficiently large then the character of the cross section at 95 MeV can change completely from forward peaked to backward peaked.

As a final exercise, Figs. 18 and 19 exhibit the differential cross sections found at 49 and 95 MeV if α_p and β_p are held fixed at their $O(Q^3)$ values, while β_n and α_n are varied with $\alpha_n + \beta_n$ constrained to the central value of Eq. (5). These plots suggest that at backward angles and higher energies the differential cross section is quite sensitive to $\alpha_n - \beta_n$.

However, significant change in the 95 MeV results presented here from those obtained at $O(Q^3)$ mandates a cautious interpretation. At the same time that the cross section at 95 MeV is more sensitive to polarizabilities than at lower energies, it is also more sensitive to $O(Q^4)$ corrections. In our view, a full $O(Q^4)$ calculation in χPT is necessary if any attempt is to be made to extract the neutron polarizability from the Saskatoon data within this framework.

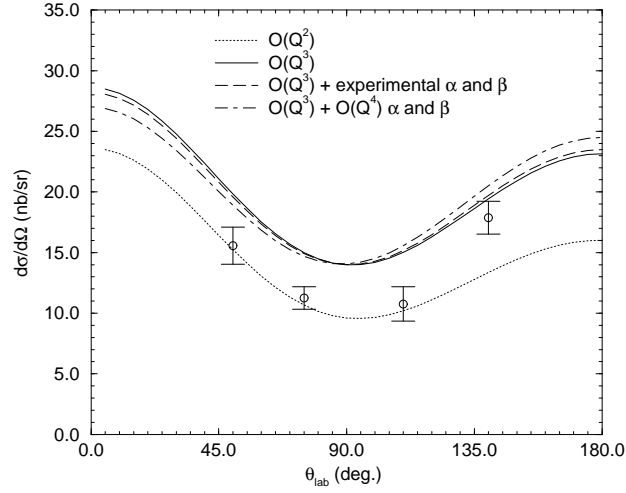


Figure 16: Results of calculations at 49 MeV using different values for the nucleon electromagnetic polarizabilities. The solid line is the result using the $O(Q^3)$ χPT value, the long-dashed line is the result using “experimental” polarizabilities, and the dot-dashed line represents a calculation with the $O(Q^4)$ polarizabilities. Experimental data from Ref. [12] also shown.

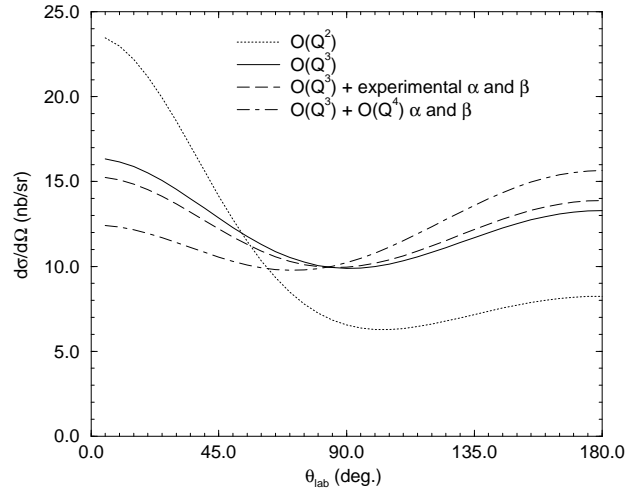


Figure 17: Results of calculations at 95 MeV using different values for the nucleon electromagnetic polarizabilities. Legend as in Figure 16.

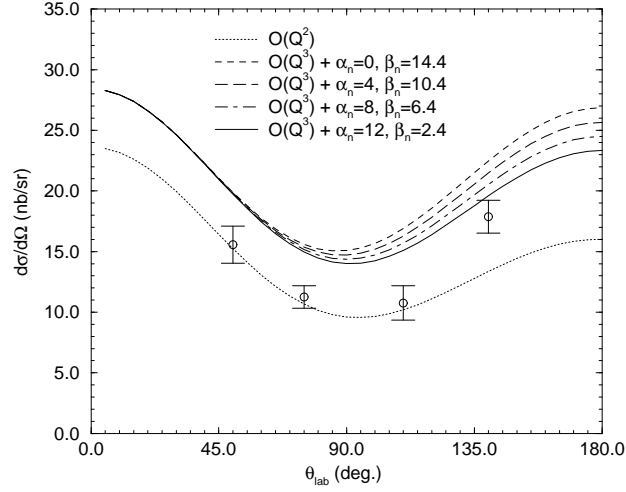


Figure 18: Results of calculations at 49 MeV which vary the neutron electric and magnetic polarizabilities while holding the sum fixed.

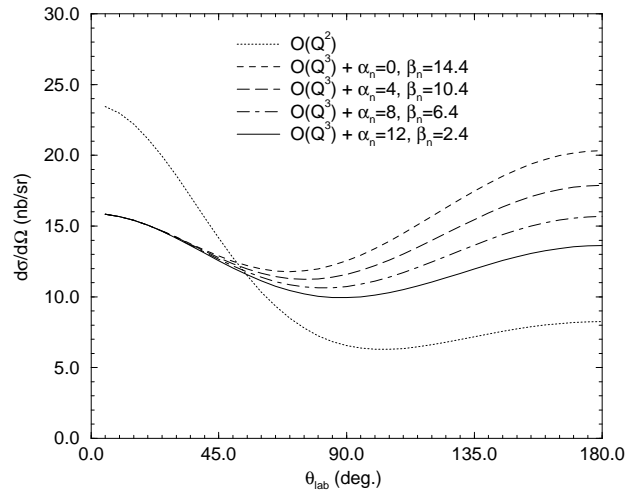


Figure 19: Results of calculations at 95 MeV which vary the neutron electric and magnetic polarizabilities while holding the sum fixed.

6 Conclusion

We have calculated the differential cross section for Compton scattering on the deuteron in χPT up to $O(Q^3)$. We have found:

- Reasonable agreement with the data at 49 MeV. At this energy $O(Q^3)$ corrections are not large compared to the leading $O(Q^2)$ result, and $O(Q^4)$ terms seem to be even smaller. There is little dependence on the wavefunction used. However, as anticipated, certain terms necessary to restore the Thomson, zero-energy, limit for photon-deuteron scattering are important at this lower energy. Once they are added to our calculation agreement with data is good.

- Good agreement with the data at 69 MeV. At this energy the convergence appears to be good. This suggests that χPT at $O(Q^3)$ is providing reasonable neutron and two-nucleon contributions.

- That the polarizability approximation should not be used in the calculation of the differential cross section at 95 MeV, since truncating the photon-nucleon amplitude at order ω^2 results in a significant change in the photon-deuteron differential cross section for forward angles.

- Wave function dependence on the order of 10% in the differential cross section. Our calculations suggest that much of this dependence would be removed if the physics of pion range were the same in both wave functions and in the computation of the kernel.

- A prediction at 95 MeV which is, however, plagued by considerable uncertainties. Convergence is slow at this energy, as indicated by the relative size of both the full set of $O(Q^3)$ corrections and a partial set of $O(Q^4)$ corrections. The cross section tends to come out somewhat smaller than at lower energies, in particular in the backward directions, although the full $O(Q^4)$ amplitude is likely to be somewhat bigger at back angles. It seems that a more stringent test of χPT at these energies—including aspects of neutron structure beyond the $O(Q^3)$ “pion cloud” picture—will have to wait for a next-order calculation.

Acknowledgements

Discussions with Jiunn-Wei Chen, Tom Cohen, Jim Friar, Harald Griesshammer, Dave Hornidge, Mark Lucas, Ulf Meißner, Martin Savage, and Roxanne Springer are gratefully acknowledged. We also thank Vincent Stoks for providing us with the Nijm93 wave function. This research was supported in part by the DOE grants DE-FG02-93ER-40762 and DE-FG03-97ER41014 and by the National Science Foundation grant PHY 94-20470. M.M would like to thank Capes and CNPq, Brazil, for support.

References

- [1] V. Bernard, N. Kaiser, and Ulf-G. Meißner, *Int. J. Mod. Phys.* **E4**, 193 (1995), [hep-ph/9501384](#).
- [2] V. Bernard, N. Kaiser, and Ulf-G. Meißner, *Phys. Rev. Lett.* **67**, 1515 (1991); *Nucl. Phys.* **B383**, 442 (1992); V. Bernard, N. Kaiser, J. Kambor, and Ulf-G. Meißner, *Nucl. Phys.* **B388**, 315 (1992).
- [3] V. Bernard, N. Kaiser, A. Schmidt, and Ulf-G. Meißner, *Phys. Lett.* **B319**, 315 (1993), [hep-ph/9309211](#); *Z. Phys.* **A348**, 317 (1994).
- [4] J. Tonnison, A. M. Sandorfi, S. Hoblit, and A. M. Nathan, *Phys. Rev. Lett.* **80**, 4382 (1998), [nucl-th/9801008](#).
- [5] A. M. Baldin, *Nucl. Phys.* **18**, 310 (1960); M. Damashek and F. Gilman, *Phys. Rev.* **D1**, 1319 (1970); D. Babusci, G. Giordano, and G. Matone, *Phys. Rev.* **C57**, 291 (1998), [nucl-th/9710017](#).
- [6] J. Schmiedmayer et al, *Phys. Rev. Lett.* **66**, 1015 (1991).
- [7] J. J. Karakowski and G. A. Miller, [nucl-th/9901018](#); J. J. Karakowski, Ph. D. thesis, University of Washington (1999), [nucl-th/9901011](#).
- [8] L. Koester et al, *Phys. Rev.* **C51**, 3363 (1995).
- [9] K. W. Rose et al, *Nucl. Phys.* **A514**, 621 (1990).
- [10] F. Wissmann, M. I. Levchuk, and M. Schumacher, *Eur. Phys. J.* **A1**, 193 (1998).
- [11] D. Drechsel, *et al.*, in *Mainz 1997, Chiral Dynamics: Theory and Experiment*, ed. A. Bernstein *et al.*, (Springer-Verlag, 1998), p. 264, [nucl-th/9712013](#).
- [12] M. Lucas, Ph. D. thesis, University of Illinois, unpublished (1994).
- [13] D. Hornidge, private communication; G. Feldman, private communication.
- [14] M. Lunding, private communication.
- [15] T. Wilbois, P. Wilhelm, and H. Arenhövel, *Few-Body Systems Suppl.* **9**, 263 (1995).
- [16] M. I. Levchuk and A. I. L'vov, [nucl-th/9809034](#), and references therein.
- [17] S. Weinberg, *Phys. Lett.* **B251**, 288 (1990); *Nucl. Phys.* **B363**, 3 (1991); *Phys. Lett.* **B295**, 114 (1992).

- [18] C. Ordóñez and U. van Kolck, Phys. Lett. **B291**, 459 (1992); U. van Kolck, Ph. D. thesis, University of Texas (1993).
- [19] U. van Kolck, Phys. Rev. **C49**, 2932 (1994).
- [20] C. Ordóñez, L. Ray, and U. van Kolck, Phys. Rev. Lett. **72**, 1982 (1994); Phys. Rev. **C53**, 2086 (1996), hep-ph/9511380.
- [21] G. P. Lepage, lectures given at the 9th Jorge Andre Swieca Summer School: Particles and Fields, Sao Paulo, Brazil, nucl-th/9706029.
- [22] *Nuclear Physics with Effective Field Theory*, ed. R. Seki, U. van Kolck, and M. J. Savage, World Scientific (1998).
- [23] U. van Kolck, in *Mainz 1997, Chiral Dynamics: Theory and Experiment*, ed. A. Bernstein *et al.*, (Springer-Verlag,1998), hep-ph/9711222; in Ref. [22]; Nucl. Phys. **A645**, 273 (1999), nucl-th/9808007.
- [24] D. B. Kaplan, M. J. Savage, and M. B. Wise, Phys. Lett. **B424**, 390 (1998); nucl-th/9801034; Nucl. Phys. **B534**, 329 (1998), nucl-th/9802075.
- [25] J.-W. Chen, H. W. Griesshammer, M. J. Savage and R. P. Springer, nucl-th/9806080; nucl-th/9809023; J.-W. Chen, nucl-th/9810021.
- [26] U. van Kolck, nucl-th/9902015.
- [27] S. R. Beane, V. Bernard, T.-S. H. Lee and Ulf-G. Meißner, Phys. Rev. **C57**, 424 (1998), nucl-th/9708035.
- [28] S. R. Beane, C. Y. Lee, and U. van Kolck, Phys. Rev. **C52**, 2914 (1995), nucl-th/9506017; S.R. Beane, V. Bernard, T.S.H. Lee, Ulf-G. Meißner and U. van Kolck, Nucl. Phys. **A618**, 381 (1997), hep-ph/9702226.
- [29] T.-S. Park, K. Kubodera, D-P. Min, and M. Rho, Phys. Rev. **C58**, 637 (1998), hep-ph/9711463.
- [30] T.-S. Park, K. Kubodera, D-P. Min, and M. Rho, astro-ph/9804144; Nucl. Phys. **A646**, 83 (1999), nucl-th/9807054.
- [31] J. L. Friar, Few-body Systems **22**, 161 (1997), nucl-th/9607020.
- [32] J. L. Friar and E. L. Tomusiak, Phys. Lett. **B122**, 11 (1983).
- [33] E. Jenkins and A. V. Manohar, Phys. Lett. **B255**, 558 (1991).

- [34] M. N Butler and M. J. Savage, Phys. Lett. **B294**, 369 (1992); T. R. Hemmert, B. R. Holstein, and J. Kambor, Phys. Rev. **D55**, 5598 (1997), [hep-ph/9612374](#); Phys. Rev. **D57**, 5746 (1998), [nucl-th/9709063](#).
- [35] D. Babusci, G. Giordano, and G. Matone, Phys. Rev. **C55**, R1645 (1997).
- [36] J. H. Koch and R. M. Woloshyn, Phys. Rev. **C16**, 1968 (1977).
- [37] R. Machleidt, K. Holinde, and Ch. Elster, Phys. Rep. **149**, 1 (1987).
- [38] V. G. J. Stoks, R. A. M. Klomp, C. P. F. Terheggen, and J. J. de Swart, Phys. Rev. **C49**, 2950 (1994), [nucl-th/9406039](#).
- [39] P. Wilhelm, Phys. Rev. **C56**, 1215 (1997), [nucl-th/9703037](#).